Myosin VIII and XI isoforms interact with *Agrobacterium* VirE2 protein and help direct transport from the plasma membrane to the perinuclear region during plant transformation

Nana Liu, Lan-Ying Lee, Yanjun Yu, and Stanton B. Gelvin*

Department of Biological Sciences, Purdue University, West Lafayette, IN 47907

*Corresponding author: Stanton B. Gelvin (gelvin@purdue.edu)

Short title: Myosins mediate plant transformation

NL, L-YL, and SBG designed the experiments; NL, L-YL, and YY carried out the experiments; NL and SBG wrote the manuscript with the help of L-YL; SBG envisaged the project and obtained funding support.

The author responsible for distribution of materials integral to the findings presented in this article in accordance with the policy described in the Instructions for Authors (https://academic.oup.com/plcell/pages/General-Instructions) is: Stanton B. Gelvin (gelvin@purdue.edu)

Authors e-mail addresses:
NL: nanaliucau@gmail.com
L-YL: lee34@purdue.edu
YY: yyj74@163.com
SBG: gelvin@purdue.edu

ABSTRACT

Virulent *Agrobacterium* strains transfer single-strand T-DNA (T-strands) and virulence effector proteins into plant cells. VirE2, one of these virulence effectors, enters the plant cell and is thought to bind T-strands, protecting them from nuclease degradation and helping guide them to the nucleus. How VirE2 is trafficked inside the plant cell is not fully understood. Using bimolecular fluorescence complementation, *in vitro* pull-down, yeast two-hybrid, and *in vivo* co-immunoprecipitation assays, we found that VirE2 binds directly to the cargo binding domains of several myosin VIII family members, and to myosin XI-K. We observed reduced susceptibility of several *Arabidopsis* actin mutants and a myosin *VIII-1/2/a/b* quadruple mutant to *Agrobacterium*-mediated transformation. Expression of cargo binding domains of myosin VIII-1, VIII-2, VIII-A, or VIII-B in transgenic plants inhibits *Arabidopsis* root transformation. However, none of the myosin VIII proteins contribute to the intracellular trafficking of VirE2. Expression of myosin *VIII-2*, *-A*, *-B*, but not *VIII-1*, cDNAs in the myosin *VIII-1/2/a/b* mutant partially restored transformation. Furthermore, functional fluorescently-tagged VirE2, synthesized in plant cells, relocalized from the cellular periphery into the cytoplasm after delivery of T-strands from *Agrobacterium*. Surprisingly, mutation of myosin *XI-k* and expression of the myosin XI-K cargo binding domain had no effect on transformation, although it blocked VirE2 movement along actin filaments. We hypothesize that myosin VIII proteins facilitate VirE2 tethering to the plasma membrane and are required for efficient localization of VirE2 to membrane sites from which they bind incoming T-strands. Myosin XI-K is important for VirE2 movement through the cytoplasm towards the nucleus.

54 **INTRODUCTION**
55
56 The soil-borne phytopathogen *Agrobacterium tumefaciens* is the causative agent of crown
57 gall disease in plants (Gelvin, 2000; Tzfira et al., 2004). The ability of *Agrobacterium* to
58 genetically transform plant cells has made *Agrobacterium*-mediated transformation the most
59 widely used platform for generating transgenic plants (Gelvin, 2017). During transformation, T-
60 DNA, a defined segment of the resident tumor inducing (Ti) plasmid, is transferred to the plant
61 cell along with several virulence (Vir) effector proteins (Bevan and Chilton, 1982). Virulence
62 effector proteins VirD5, VirE2, VirE3, and VirF, along with VirD2, which covalently links to T-
63 strands (single-strand T-DNA molecules), are transferred from *Agrobacterium* to the plant
64 through a type IV secretion system (T4SS) (Cascales and Christie, 2004; Christie et al., 2005).
65 VirE2, the most abundant of the virulence effector proteins (Engstrom et al., 1987), is
66 important for efficient plant transformation as *virE2* mutant *Agrobacterium* strains are highly
67 attenuated in virulence (Stachel and Nester, 1986; Rossi et al., 1996). *In vitro*, VirE2 binds to
68 single-strand (ss)DNA in a sequence-independent manner and has been proposed to interact with
69 single-strand T-strands, linked to VirD2, in the plant cytoplasm, forming a "T-complex" and
70 protecting T-strands from nuclease degradation (Citovsky et al., 1989; Sen et al., 1989; Howard
71 et al., 1990; Yusibov et al., 1994; Rossi et al., 1996; Gelvin, 1998). VirE2 does not interact with
72 T-strands in *Agrobacterium* (Cascales and Christie, 2004) and its interaction with T-strands to
73 form a T-complex *in planta* has only been inferred. In addition to its *in vitro* DNA binding
74 activity, VirE2 can form membrane channels which permit the transport of ssDNA through
75 artificial membranes (Dumas et al., 2001; Duckely et al., 2005). Recent research showed that
76 VirE2 is anchored on the host plasma membrane through interaction with VirE3 at
77 *Agrobacterium*-host contact sites. Such membrane associations may facilitate the proposed
78 interactions between VirE2 and T-strands as the T-strands enter the plant cell (Li et al., 2018).
79 Efficient plant transformation by a *virE2* mutant *Agrobacterium* strain (the "T-DNA donor")
80 can be restored by co-inoculation with a bacterial strain lacking T-DNA but expressing VirE2
81 (the "VirE2 donor"; Otten et al., 1984; Citovsky et al., 1992; Simone et al., 2001), and a *virE2*
82 mutant *Agrobacterium* strain can be complemented to full virulence by expression of a *VirE2*
83 transgene *in planta* (Citovsky et al., 1992; Lapham et al., 2021), indicating that VirE2 is
84 functional in plants during transformation. However, the subcellular localization of VirE2
85 remains controversial. Early reports demonstrated nuclear localization of VirE2 (Citovsky et al.,

86 1992), but other studies from several laboratories indicated that VirE2 localizes in the cytoplasm
87 (Gelvin, 2010). A recent report claimed that a small amount of VirE2 can enter the nucleus, but
88 only in the presence of VirD2 and T-strands (Li et al., 2020). How VirE2, and potentially
89 associated T-strands, are trafficked from their entry point at the cell periphery to the nucleus
90 remains unknown.
91 Myosins, motor proteins that convert chemical energy into directed movement of cargo
92 proteins along actin filaments, are key players in trafficking proteins and organelles in plants
93 (Vale, 2003; Richards and Cavalier-Smith, 2005). Two classes of myosins, myosin VIII and XI,
94 are encoded by plant genomes. *Arabidopsis thaliana* encodes 13 myosin XI group members and
95 four myosin VIII group members (Bezanilla et al., 2003; Foth et al., 2006). Generally, myosin
96 proteins contain a highly conserved N-terminal motor domain for actin binding, a neck domain
97 with a number of IQ repeats for light-chain binding, a coiled-coil domain that is responsible for
98 myosin protein dimerization, and a specific C-terminal tail domain that binds cargo (Trybus,
99 2008). Class XI myosins, known as organelle transporters, colocalize with organelles and are
100 involved in the rapid trafficking of Golgi stacks, streaming of endoplasmic reticulum (ER), and
101 cellular remodeling (Lee and Liu, 2004; Reisen and Hanson, 2007; Avisar et al., 2008b; Sparkes
102 et al., 2009; Ueda et al., 2010). In addition, myosins XI-K and XI-2 play major and overlapping
103 roles in root hair development (Peremyslov et al., 2008). In contrast to class XI myosins,
104 considerably less is known about the intracellular functions of class VIII myosins. Class VIII
105 myosins colocalize with plasmodesmata, the endoplasmic reticulum, and the plasma membrane
106 (Golomb et al., 2008) and may function in intercellular protein and RNA delivery to the
107 plasmodesmata, in endocytosis, and in anchoring actin filaments at plasmodesmata sites
108 (Reichelt et al., 1999; Wojtaszek et al., 2005; Avisar et al., 2008a; Golomb et al., 2008;
109 Sattarzadeh et al., 2008). Moreover, myosin VIII is important for the cell-to-cell movement of
110 virus proteins, and is required for viral movement protein targeting to and virus trafficking
111 through plasmodesmata (Amari et al., 2014).
112 The actin cytoskeleton functions to organize the endomembrane system and trafficking
113 patterns within the cell (Smith and Oppenheimer, 2005; Hussey et al., 2006). Cargo-binding and
114 intracellular transport by myosin is proposed to exert force on the actin filaments (Staiger et al.,
115 2009). Yang et al. (2017) reported that trafficking of VirE2 inside plant cells is powered by
116 myosin XI-K via the endoplasmic reticulum and F-actin filaments. However, our knowledge of

117 the roles of plant myosins in specific steps of VirE2 trafficking and transformation remains
118 sparse. In the present study, we investigated the roles of myosin VIII family members and
119 myosin XI-K in *Agrobacterium*-mediated transformation and in VirE2 intracellular movement.
120 Using a dominant-negative approach by overexpressing individual myosin cargo-binding
121 domains, and by overexpressing various individual full-length myosin cDNAs, we show that
122 *Arabidopsis* myosins VIII-2, VIII-A, and VIII-B, but not XI-K, are important for transformation.
123 These three myosin VIII isoforms interact with VirE2 and retain it at the periphery of root cells.
124 When T-DNA enters the plant cell, a portion of peripherally localized VirE2 relocalizes into the
125 cytosol, especially the perinuclear region. However, class VIII myosins do not affect the
126 movement of VirE2 along actin filaments within the cytoplasm. In contrast, myosin XI-K
127 supports the intracellular movement of VirE2. We propose that myosins VIII-2, VIII-A, and
128 VIII-B tether VirE2 to the plasma membrane. Entry of VirD2/T-strands into the plant cell
129 releases VirE2 from the membrane, following which VirE2 translocates to the perinuclear region
130 along actin filaments, powered by myosin XI-K.
131

132 **RESULTS**

133 **The actin cytoskeleton is important for *Agrobacterium*-mediated transformation**

134 The actin cytoskeleton is conserved in diverse eukaryotic organisms and is important for a
135 variety of plant developmental and other processes, including cell growth, division, and
136 expansion; organelle motility; organization of the cellular interior; endomembrane trafficking;
137 and host defense responses (Smith and Oppenheimer, 2005; Embley and Martin, 2006; Hussey et
138 al., 2006; Szymanski and Cosgrove, 2009; Peremyslov et al., 2010). To test whether the actin
139 cytoskeleton plays a role in *Agrobacterium*-mediated transformation, we conducted transient and
140 stable *Arabidopsis* root transformation assays using wild-type plants and plants individually
141 mutant in two root-expressed actin genes, *actin2* (*act2*) and *actin7* (*act7*). These actin mutant
142 plants showed substantial reductions (three- to five-fold) in transformation. Introduction of a
143 wild-type *Act7* cDNA into the *act7-4* mutant restored both transient and stable transformation
144 (Figure 1A). These results show that root-expressed actin genes are important for transformation
145 of *Arabidopsis* roots. We also conducted root transformation assays using a mutant of the
146 pollen-expressed *actin12* gene (*act12*) and the *botero* (*bot1*) mutant that shows disorganization

147 of the root cortical microtubule network (Bichet et al., 2001). These mutants showed wild-type
148 levels of transformation (Figure 1A), indicating that neither a pollen-expressed actin gene nor the
149 correct organization of root microtubules is essential for *Agrobacterium*-mediated root
150 transformation.

151 Yang et al. (2017) showed that the *Agrobacterium* virulence effector protein VirE2 uses
152 myosin XI-K to traffic through the tobacco cytoplasm. Given the importance of VirE2 for
153 transformation, we individually tested *Arabidopsis* mutants in each of the 13 myosin XI and four
154 myosin VIII gene family members for their susceptibility to transient and stable *Agrobacterium*-
155 mediated transformation. Figures 1B and C, and Supplemental Figure S1, show that apart from
156 the *myosin XI-h* mutant, mutation of no other single myosin gene affected transformation. In
157 particular, mutation of the *myosin XI-k* gene did not decrease transformation. Because of
158 potential functional redundancy among the plant myosin VIII and XI family members
159 (Prokhnevsky et al., 2008), we also tested several higher order myosin VIII and myosin XI
160 mutants. Higher order *myosin XI-k* mutants (*XI-k/i*, *XI-k/1/2*, and *XI-k/1/2/i*) showed decreased
161 transformation susceptibility (Figures 1B and 1C). Similarly, the higher order myosin VIII
162 mutants *1/a*, *2/b*, *1/2/a*, and *1/2/a/b* showed reduced transformation susceptibility compared to
163 wild-type Col-0 plants (Figures 1B and 1C).

164 We compared root and above-ground plant growth of each of the higher order myosin XI and
165 myosin VIII mutants. Similar to what was previously observed (Ojangu et al., 2007; Peremyslov
166 et al., 2008), the myosin *XI-k/1/2/i* quadruple mutant displayed a strong growth and
167 developmental phenotype compared with Col-0 plants: the main roots had fewer lateral branches
168 and shorter root hairs, and the plants were dwarf. However, the myosin *VIII 1/2/a/b* quadruple
169 mutant appeared similar to Col-0 plants in growth, root development, and the ability to form calli
170 from cut root segments (Supplemental Figures S2A and S2B). Roots and the crown of the plant
171 are the natural target tissues for *Agrobacterium*-mediated transformation. Because we were
172 conducting quantitative root transformation assays (Gelvin, 2006), we did not continue to
173 investigate transformation susceptibility of the abnormal roots of the myosin *XI-k/1/2/i* quadruple
174 mutant. We therefore turned our attention to investigating the importance of the various myosin
175 VIII isoforms for transformation, and to the myosin XI-K protein.
176

177 **Expression of full- length myosin *VIII-2*, *VIII-A*, and *VIII-B* cDNAs, but not a myosin *VIII-***
178 ***1* cDNA, increases susceptibility of the myosin *VIII-1/2/a/b* quadruple mutant to**
179 ***Agrobacterium*-mediated transformation**

180 To determine the importance of each *myosin VIII* gene for *Agrobacterium*-mediated root
181 transformation, we individually expressed cDNAs for each *myosin VIII* gene in the *myosin VIII-*
182 *1/2/a/b* quadruple mutant. We placed each *myosin VIII* cDNA under the control of a strong
183 Cauliflower Mosaic Virus (CaMV) double 35S promoter (hereafter reported in Supplemental
184 Table 1 as the *Agrobacterium* strains used to make the transgenic lines; At2361-At2164; At2360
185 was used as an empty vector control) or a β-estradiol-inducible promoter (Zuo et al., 2000;
186 At2389-2392) and generated multiple transgenic lines. Because of the importance of myosins in
187 trafficking molecules and organelles through the plant cytoplasm (Avisar et al., 2008b), we
188 hereafter limited our transformation assays to transient transformation which measures T-DNA
189 and virulence effector protein movement through the cytoplasm, entry into the nucleus, and
190 expression of non-integrated transgenes. Thus, these assays predominantly measure non-
191 integrated transgenes.

192 Transient root transformation assays of five independent transgenic lines of each *myosin VIII*
193 cDNA indicated that individual expression of the *myosin VIII-2*, *VIII-A*, and *VIII-B* cDNAs
194 increased the transformation susceptibility of the *myosin VIII-1/2/a/b* quadruple mutant (Figure
195 2A and Supplemental Figures S3B-D), indicating a role for these myosins in *Agrobacterium*-
196 mediated transformation. However, expression of the *myosin VIII-1* cDNA in the quadruple
197 mutant background did not increase transformation susceptibility (Figure 2A and Supplemental
198 Figure S3A). This latter result suggests either that myosin VIII-1 does not contribute to
199 transformation or that expression of myosin VIII-1 is not sufficient to increase transformation in
200 the absence of the other three myosin VIII isoforms. To distinguish between these two
201 possibilities, we individually overexpressed each *myosin VIII* cDNA in wild-type Col-0 plants.
202 Interestingly, overexpression of the *myosin VIII-1* cDNA, but not the *myosin VIII-2*, *VIII-A*, or
203 *VIII-B* cDNAs, increased susceptibility of Col-0 plants to *Agrobacterium*-mediated
204 transformation (Figure 2B and Supplemental Figures S3A-D). These results indicate that myosin
205 VIII-1 can contribute to transformation, but that expression of myosin VIII-1 is not sufficient to
206 alter transformation susceptibility in the absence of the other myosin VIII isoforms. Transgenic

207 plants harboring inducible *myosin VIII* cDNAs yielded results similar to that of plants
208 constitutively expressing these cDNAs (Supplemental Figures S4A-D).
209 Finally, we generated transgenic lines that expressed two *myosin VIII* cDNAs (*VIII-A* and
210 *VIII-B* [At2375], or *VIII-2* and *VIII-B* [At2376]) in both the *myosin VIII-1/2/a/b* quadruple
211 mutant (Figure 2C) and in wild-type Col-0 plants (Figure 2D). Overexpression of these two sets
212 of myosin cDNAs did not increase transformation of otherwise wild-type plants. However,
213 expression of these pairs of myosin cDNAs in the *myosin VIII-1/2/a/b* quadruple mutant
214 enhanced transformation to a greater extent than did expression of these cDNAs individually
215 (Figures 2C and Supplemental Figures S5A-D). These results indicate that *myosin VIII-A*, *VIII-*
216 *B*, and *VIII-2* genes contribute synergistically to transformation. These results further suggest
217 that the level of expression of the *myosin VIII-2*, *VIII-A*, and *VIII-B* genes in wild-type roots is
218 sufficient for maximal transformation, and that increasing expression of these genes cannot
219 further increase transformation.

220 **Inducible expression of *myosin VIII*, but not *myosin XI-K*, cargo binding domain transgenes**
221 **affects *Agrobacterium*-mediated transient root transformation**

222 Yang et al. (2017) demonstrated that expression of a myosin XI-K cargo binding (globular tail)
223 domain inhibited VirE2 movement in tobacco leaf cells. To determine whether specific myosin
224 VIII members are important for *Agrobacterium*-mediated transformation using a similar
225 dominant-negative approach, we generated transgenic *Arabidopsis* lines individually expressing
226 cDNAs encoding each of the four myosin VIII cargo binding domains (CBD; At2315-2318), or
227 the myosin XI-K CBD (At2319), under the control of a β-estradiol inducible promoter. Because
228 these CBD constructs lack the myosin motor domain, they are not able to transport their cargoes
229 along actin filaments. We tested the susceptibility of 3-4 independent transgenic lines for each
230 CBD construct to *Agrobacterium*-mediated transient transformation, either after 24 hr transgene
231 induction or without induction. Induction of each of the four *myosin VIII* CBD transgenes
232 decreased transformation two- to three-fold, whereas induction of the *myosin XI-K* CBD
233 transgene had no significant effect on transformation (Figure 3 and Supplemental Figures S6A-
234 E). These data further suggest that the four myosin VIII proteins contribute to *Agrobacterium*-

235 mediated transformation, whereas myosin XI-K is not required for transformation. However,
236 below we show that myosin XI-K is important for VirE2 movement through the cytoplasm.

237 **Myosin VIII proteins are required for *Arabidopsis* roots expressing VirE2 to complement**
238 **the virulence of a *virE2* mutant *Agrobacterium* strain, and to mitigate VirE2 aggregation**

239 *Agrobacterium virE2* mutants are severely debilitated in virulence (Rossi et al., 1996). However,
240 expression of VirE2 or VirE2-Venus transgenes in plants restores virulence, indicating that the
241 major role of VirE2 in transformation occurs in the plant (Citovsky et al., 1992; Lapham et al.,
242 2021). To determine the importance of myosin VIII proteins for such "*in planta*"
243 complementation, we generated numerous *Arabidopsis* transgenic lines expressing a *VirE2-*
244 *Venus* transgene, under the control of a β-estradiol-inducible promoter, in both wild-type and in
245 *myosin VIII* quadruple mutant plants. Twenty four hr after incubation of roots of these lines in
246 medium with or without inducer, we cut the roots into small segments and infected them with *A.*
247 *tumefaciens* At1879 (lacking a *virE2* gene) containing the T-DNA binary vector pBISN2 with a
248 *gusA*-intron gene in the T-DNA (Narasimhulu et al., 1996). Six days later we assessed transient
249 transformation efficiency by conducting β-glucuronidase (GUS) activity assays using the
250 chromogenic substrate 5-bromo-4-chloro-3-indolyl-β-D-glucuronide (X-gluc). As previously
251 reported (Lapham et al., 2021), induction of the *VirE2-Venus* transgene in wild-type Col-0 plants
252 complemented the loss of VirE2 function when a *virE2 Agrobacterium* mutant was used.
253 However, induction of the *VirE2-Venus* transgene in *myosin VIII* quadruple mutant plants could
254 not compensate the loss of VirE2 function when a *virE2 Agrobacterium* mutant was used
255 (Figures 4A and 4B). Thus, *Myosin VIII* expression is required for *in planta* complementation of
256 an *Agrobacterium virE2* mutant.
257 VirE2 usually localizes in the plant cytoplasm, although in the presence of the virulence
258 effector protein VirD2 and T-strands a small amount may enter the nucleus (Gelvin, 2010; Li et
259 al., 2020). To determine whether myosin VIII affects the subcellular distribution of VirE2, we
260 used confocal microscopy to visualize β-estradiol induced VirE2-Venus in both the Col-0 and
261 *myosin VIII* quadruple mutant backgrounds containing an inducible *VirE2-Venus* transgene.
262 VirE2 is known to aggregate both *in vitro* and in plants (Bhattacharjee et al., 2008; Dym et al.,
263 2008). Under our induction conditions VirE2-Venus showed a pattern of aggregation in the

264 *myosin VIII* quadruple mutant distinct from that seen in the Col-0 background. In roots of the
265 quadruple mutant, VirE2-Venus aggregated to a greater extent than it did in wild-type roots
266 (Figure 4C). The sizes of VirE2 aggregates from two random areas of each of six images were
267 measured and the average sizes were calculated. The average VirE2 aggregate size in root cells
268 of the *myosin VIII* quadruple mutant was 6.2±0.6 μm^2, compared to an average aggregate size of
269 2.0±0.3 μm^2 in wild-type roots (Figure 4D). Furthermore, the total cellular area occupied by
270 these VirE2 aggregates was greater in root cells of the *myosin VIII* mutant (17.0±1.1%) than in
271 similar wild-type cells (4.7±0.9%) (Figure 4D). To determine whether this extensive VirE2
272 aggregation in myosin *VIII* mutant cells resulted from higher levels of VirE2-Venus expression
273 in roots, we extracted total proteins from β-estradiol-induced roots of these plants and
274 determined the relative amounts of VirE2-Venus expressed in roots using anti-GFP antibodies.
275 As a loading control for the protein blots, we used an antibody targeting the house-keeping
276 protein phosphoenolpyruvate carboxylase (PEPC). Strikingly, myosin *VIII* quadruple mutant
277 roots express, on average, less VirE2-Venus than do wild-type roots (Figure 4E). Therefore, the
278 more extensive aggregation of VirE2-Venus in *myosin VIII* mutant roots is unique and cannot be
279 explained by greater accumulation of this protein.
280 To determine which myosin protein influences VirE2-Venus aggregation, we generated
281 numerous transgenic *Arabidopsis* lines (using *Agrobacterium* strains At2315-At2319), in the
282 *myosin VIII* quadruple mutant background, expressing both VirE2-Venus and individual
283 *mCherry-myosin VIII CBD* cDNAs under the control of a β-estradiol-inducible promoter.
284 Following induction, we measured the size of the VirE2-Venus aggregates in root cells and the
285 percentage of root cell volume taken up by these aggregates. Figures 5A and 5B show that,
286 compared to expression of VirE2-Venus in the absence of expression of a myosin CBD
287 transgene, expression of myosin VIII-A, VIII-B, and VIII-2 CBDs reduced both the size of
288 VirE2-Venus aggregates (from 7.5±1.9 μm^2 down to 2.4±0.3 μm^2, 3.7±0.5 μm^2, and 3.1±0.3
289 μm^2, respectively) and the percentage of the cell volume (from 17.7±2.0% down to 3.6±0.6%,
290 6.3±0.4%, and 6.1±0.5%, respectively) occupied by these aggregates, due to their dominant
291 negative effects. However, the CBD of myosin VIII-1 did not substantially reduce aggregate
292 size or the percentage of the cell volume occupied by the aggregates (Figure 5A): the average
293 aggregates size was 6.7±0.7 μm^2, and the percentage of the cell volume was 11.8±1.1%. These

294 results suggest that myosin VIII-A, VIII-B, and VIII-2 CBDs interact with VirE2 in plant cells
295 and that the myosin VIII-1 CBD may fundamentally differ from the CBDs of the other three
296 myosin VIII members.

297 **VirE2 interacts directly with some, but not all, myosin VIII cargo binding domains and**
298 **with the CBD of myosin XI-K**

299 Because myosin VIII proteins are required for VirE2 to function in virulence, and because
300 myosin VIII CBD expression affects the degree to which VirE2 aggregates *in planta*, we
301 investigated whether myosin protein cargo binding domains interact with VirE2. We first tested
302 the direct interaction of VirE2 with each of the myosin VIII and the myosin XI-K protein CBDs
303 using an *in vitro* pull-down assay. We individually incubated recombinant VirE2-Venus with
304 recombinant myc-tagged myosin CBDs. As a control, we substituted recombinant Venus protein
305 for VirE2-Venus. As further controls, we incubated VirE2-Venus with myc-tagged VIP1, a
306 protein known to interact with VirE2 (Tzfira et al., 2001; Djamei et al., 2007), or myc-tagged
307 Lamin C, a protein known not to interact with VirE2 (Ueki and Citovsky, 2005). We captured
308 VirE2-Venus, or Venus, and any interacting proteins on anti-GFP antibody beads, subjected the
309 bound proteins to SDS gel electrophoresis, then conducted Western blot analysis using anti-myc
310 antibodies. Figures 6A-F show that the CBDs of myosins VIII-A, VIII-B, VIII-2, and XI-K
311 directly interacted with VirE2-Venus, but not with Venus. However, we were not able to detect
312 interaction of VirE2-Venus with the CBD of myosin VIII-1. As expected, VirE2-Venus
313 interacted with myc-tagged VIP1 but not with myc-tagged Lamin C (Figure 6). These data were
314 confirmed using a yeast two-hybrid system. VirE2 interacted in yeast with the CBDs of myosins
315 VIII-A, VIII-B, VIII-2, and XI-K, as well as with VIP1. However, VirE2 did not interact in
316 yeast with the CBD of myosin VIII-1 or with the negative control Lamin C (Figures 7A and 7B).
317 To assess the interactions of VirE2 with myosin VIII or XI-K CBD proteins *in vivo*, we
318 conducted co-immunoprecipitation experiments using transgenic *Arabidopsis* roots expressing
319 VirE2-Venus and, individually, each of the myc-tagged myosin VIII or the myosin XI-K CBDs.
320 Using anti-GFP antibody beads to capture VirE2-Venus and associated proteins followed by
321 immunoblotting using anti-myc tag antibody to detect CBDs, we observed robust co-
322 immunoprecipitation between VirE2-Venus and the myosin VIII-2, VIII-A, VIII-B, and XI-K

323 CBDs (~4% of the input myc-myosin VIII-2, VIII-A, VIII-B, and XI-K CBDs were co-
324 immunoprecipitated with anti-GFP antibody). However, we also observed some co-
325 immunoprecipitation between VirE2 and the myc-tagged myosin VIII-1 CBD (~1.6-2% of the
326 input myosin VIII-1 CBD; Figures 8A and 8B). As expected, VirE2-Venus interacted with VIP1
327 (Figure 8A), and the myosin VIII-2 CBD did not interact with the control Venus protein (Figure
328 8B). The *in vivo* co-immunoprecipitation of VirE2-Venus with the myosin VIII-2, VIII-A, VIII-
329 B, and XI-K CBDs recapitulated the *in vitro* interaction and yeast two-hybrid results. However,
330 *in vivo* co-immunoprecipitation of the myosin VIII-1 CBD with VirE2-Venus, in the absence of
331 interaction *in vitro* and in yeast, suggests that this *in vivo* interaction may be indirect and
332 mediated by other factors within *Arabidopsis* roots.

333 **VirE2 and Myosin VIII proteins co-localize at the cell periphery**

334 The vast majority of VirE2 protein localizes within the cellular cytoplasm, and in wild-type
335 *Arabidopsis* roots is often found in the peripheral regions of the cell (Shi et al., 2014). VirE2 has
336 been proposed to form membrane channels through which VirD2/T-strands translocate from
337 *Agrobacterium* into the plant cell (Dumas et al., 2001; Duckely et al., 2005). Myosin VIII
338 proteins also localize to the plasma membrane (Golomb et al., 2008). To determine whether
339 VirE2 and full-length myosin proteins co-localize at the cell periphery, we generated transgenic
340 *Arabidopsis* plants expressing VirE2-Venus and various mCherry-tagged full-length myosin
341 protein cDNAs under the control of a β-estradiol inducible promoter (using *Agrobacterium*
342 strains At2447-At2450) in the Col-0 background. After β-estradiol induction, we imaged roots
343 using confocal microscopy (Figure 9). Myosins VIII-1, VIII-A, and VIII-B localized mostly to
344 the cellular periphery, whereas myosin VIII-2 localized both to the cellular periphery and to the
345 nucleus. All myosin VIII and XI-K proteins also localized throughout the cytoplasm.
346 We also determined whether VirE2 and myosin cargo binding domains co-localize at the cell
347 periphery. We similarly generated transgenic *Arabidopsis* plants expressing VirE2-Venus and
348 various mCherry-tagged myosin CBD cDNAs under the control of a β-estradiol inducible
349 promoter (using *Agrobacterium* strains At2315-At2319). After β-estradiol induction, we imaged
350 roots using confocal microscopy (Figures S10A and S10B). The CBDs of myosins VIII-A and
351 VIII-2 localized almost exclusively to the cellular periphery, whereas the CBD of myosin VIII-B

352 localized both to the cellular periphery and to the nucleus (Figure S10A). The myosin VIII-1
353 and XI-K CBDs localized not only at the cellular periphery but also throughout the cytoplasm
354 (Figure S10A).
355 When co-expressed in the Col-0 background, VirE2 and the myosin VIII-2, VIII-A, VIII-B,
356 and XI-K CBDs partially co-localized at the cell periphery (Pearson's correlation coefficient =
357 0.56±0.04, 0.68±0.05, 0.63±0.04, and 0.69±0.03, respectively; overlap coefficient = 0.65±0.03,
358 0.72±0.06, 0.70±0.03, and 0.77±0.04, respectively; Figure S10B). However, co-localization of
359 VirE2 with the myosin VIII-1 CBD at the cell periphery was less extensive (Pearson's
360 correlation coefficient = 0.44±0.03; overlap coefficient = 0.48±0.01; Figure S10B). Staining
361 VirE2-Venus expressing *Arabidopsis* roots with the plasma membrane dye FM4-64 revealed that
362 VirE2 localized near to but not in the plasma membrane (Pearson's correlation coefficient =
363 0.42±0.07; overlap coefficient = 0.45±0.03; Supplemental Figures S7A and B). However, in the
364 myosin VIII quadruple mutant background, VirE2 localized less extensively at the cellular
365 periphery and more within the general cytoplasm (Supplemental Figures S8A and B). Co-
366 expression of mCherry-myosin VIII-1, VIII-A, or VIII-2 CBDs with the plasma membrane
367 marker PIP2A-Venus (using *Agrobacterium* strains At2370, At2371, and At2374, respectively)
368 revealed that these myosin VIII CBDs co-localize with PIP2A (Supplemental Figures S9A-C),
369 similar to what has previously been reported (Golomb et al., 2008).
370 Taken together, these results suggest that the myosin VIII-2, VIII-A, and VIII-B full-length
371 proteins and their respective CBDs localize to the plasma membrane where they may temporarily
372 tether VirE2.

373 **VirE2 and several myosin VIII full-length proteins interact at the cell periphery**

374 In order to test whether VirE2 may be a cargo of myosin VIII proteins, we conducted
375 bimolecular fluorescence complementation (BiFC) assays to visualize *in planta* protein-protein
376 interactions. We generated transgenic *Arabidopsis* plants expressing VirE2-cYFP and nVenus-
377 tagged full-length myosin protein cDNAs under the control of a β-estradiol inducible promoter
378 (using *Agrobacterium* strains At2443-At2446). The plants also constitutively expressed
379 mCherry-actin binding domain 2 (ABD2) as an actin marker. After inducing the plants with β-
380 estradiol, we detected YFP fluorescence mainly at the cellular periphery of root cells when

381 VirE2-cYFP was co-expressed with the nVenus-tagged myosins VIII-2, VIII-A, or VIII-B, but
382 no fluorescence with myosin VIII-1 (Figure 10), indicating a lack of direct interaction with the
383 myosin VIII-1 protein. These results again suggest that the CBDs of myosin VIII-2, VIII-A, and
384 VIII-B may temporarily tether VirE2 to the plasma membrane.
385 We similarly conducted bimolecular fluorescence complementation (BiFC) assays to
386 visualize *in planta* protein-protein interactions between VirE2 and myosin cargo binding
387 domains. We generated transgenic *Arabidopsis* plants expressing VirE2-cYFP and nVenus-
388 tagged myosin CBD cDNAs under the control of a β-estradiol inducible promoter (using
389 *Agrobacterium* strains At2320-At2324). The plants also constitutively expressed mCherry-actin
390 binding domain 2 (ABD2) as an actin marker. After inducing the plants with β-estradiol, we
391 detected YFP fluorescence mainly at the cellular periphery of root cells when VirE2-cYFP was
392 co-expressed with the nVenus-tagged CBDs of myosins VIII-A, VIII-B, VIII-2, or myosin XI-K,
393 but no fluorescence with the myosin VIII-1 CBD (Figure S11), indicating a lack of direct
394 interaction. VirE2-cYFP additionally interacted with the CBD of myosin XI-K in the
395 cytoplasm. VirE2-cYFP did not interact with the negative control protein Lamin C. These
396 results again suggest that the CBDs of myosin VIII-2, VIII-A, VIII-B, and XI-K may temporarily
397 tether VirE2 to the plasma membrane, but that only myosin XI-K may transport VirE2 along
398 actin filaments through the cytoplasm.
399
400 **Some VirE2 molecules re-localize to the perinuclear region during infection by a virulent**
401 ***Agrobacterium* strain**
402 Some VirE2-Venus fluorescence, when constitutively expressed in *Arabidopsis* roots, localizes
403 at the cellular periphery, especially at the cell poles (Shi et al., 2014; Li et al., 2020). Li et al.
404 (2020) showed that during agroinfiltraion, a small amount of VirE2 can enter the nucleus of
405 tobacco leaf cells, and this entry requires the presence of VirD2 and T-strands. To determine
406 whether transgenically-expressed VirE2 also relocalizes to the nucleus in the presence of VirD2
407 and T-strands, we incubated *Arabidopsis* roots containing an inducible *VirE2-Venus* transgene
408 with β-estradiol. After 24 hr, we infected root segments with a *virE2*-deletion *Agrobacterium*
409 strain either lacking T-DNA (At2403; no binary vector) or containing T-DNA on a binary vector
410 (At2404). Twenty-four hours after inoculation, we observed VirE2-Venus subcellular
411 localization by confocal microscopy. Root segments infected by *A. tumefaciens* At2403 did not

412 show altered VirE2-Venus subcellular localization: fluorescence was distributed throughout the
413 cytoplasm, including at the cellular periphery (Supplemental Figure S12A). However, infection
414 by *A. tumefaciens* At2404 resulted in a partial redistribution of VirE2-Venus within the
415 cytoplasm: fluorescence increased in the perinuclear area (Supplemental Figure S12B).
416 Quantitative analysis of fluorescence intensity showed that perinuclear VirE2 increased ~5-fold
417 in the presence of T-DNA (Figure 11A). However, we were unable to detect VirE2-Venus
418 within the nucleus. These data suggest that the transfer of T-DNA to plant cells results in a
419 partial redistribution of VirE2 to the area surrounding the nucleus.

420 **T-strands delivered by *Agrobacterium* can relocalize VirE2 from the cellular periphery into**
421 **the cytosol**

422 Because much VirE2 produced *in planta* is already in the general cell cytosol, the data presented
423 in Figure 11A and the movies in Supplemental Figure S13 were not able to show redistribution
424 of VirE2-Venus specifically from the cell periphery into the perinuclear area. We therefore
425 conducted the VirE2-Venus re-localization experiments, following *Agrobacterium* infection, on
426 root segments overexpressing the various myosin VIII or myosin XI-K CBDs. We reasoned that
427 when most VirE2-Venus is tethered to the plasma membrane by myosin VIII-A, VIII-B, VIII-2,
428 and (to a lesser extent) XI-K, as seen in Supplemental Figure 10A, we may be able to detect re-
429 distribution to VirE2-Venus more easily when T-strands are introduced into the cells by
430 *Agrobacterium*.
431 We generated transgenic plants expressing VirE2-Venus and individual myc-tagged myosin
432 CBD cDNAs (using *Agrobacterium* strains At2423-At2427), both under the control of a β-
433 estradiol-inducible promoter. After inducing the transgenes for 24 hr, we infected root segments
434 with *virE2* mutant *Agrobacterium* strains lacking or containing a T-DNA binary vector. The
435 bacteria (At2403 and At2404, respectively) additionally contained a plasmid expressing mCherry
436 to mark the location of the bacteria during infection. We observed fluorescence by confocal
437 microscopy eight hours after infection and calculated the percentage of fluorescence shift
438 between the cell periphery and the cytosol. When At2404, capable of transferring T-DNA, was
439 used, some of the VirE2-Venus fluorescence signal re-localized from the cell periphery into the
440 cytoplasm when plants expressed the myosin VIII-A, VIII-B, or VIII-2 CBDs (Figures 11C,

441 11D, and 11E, respectively, and movies in Supplemental Figures S15-17). No such
442 redistribution of the VirE2-Venus signal was observed when we infected roots with a strain,
443 At2403, lacking T-DNA. The distribution of VirE2-Venus signal was not altered in roots
444 infected with *A. tumefaciens* At2404 and expressing the CBDs of myosins VIII-1 or XI-K
445 (Figures 11 B and F; movies in Supplemental Figures S14 and S18). These results further
446 suggest that myosins VIII-A, VIII-B, and VIII-2 may temporarily tether VirE2 at the cell
447 periphery. However, upon transfer of T-DNA into the cell, VirE2 is released into the cellular
448 interior.
449
450 **Following T-DNA transfer, VirE2 moves from the cellular periphery to the interior along**
451 **actin filaments**
452 To address whether VirE2-Venus moves along actin filaments, we used *Arabidopsis* transgenic
453 lines expressing inducible VirE2-Venus and myc-tagged myosin VIII CBD cDNAs, and
454 expressing mCherry-ABD2 to mark actin filaments (using *Agrobacterium* strains At2365-
455 At2369). Time-lapse imaging of control plants, which expressed VirE2-Venus and mCherry-
456 ABD2 but without any myosin CBD, indicated that some VirE2-Venus moves along actin
457 filaments at a velocity of 0.353±0.06 μm/sec (Figure 12). In the presence of any of the four
458 myosin VIII CBDs, the velocity of VirE2-Venus along actin filaments in leaf or root cells
459 remained unchanged (Table 1). Additionally, the velocity of VirE2-Venus movement along
460 actin filaments was not altered in the *myosin VIII-1/2/a/b* quadruple mutant (Figure 12, Table 1).
461 However, when the myosin XI-K CBD was expressed in the plant, no VirE2 movement was
462 detected in either leaf or root cells. These results indicate that only myosin XI-K, but not myosin
463 VIII proteins, are important for VirE2 trafficking through leaf and root cells.
464 To test if the blockage of VirE2-Venus movement along actin filaments by the myosin XI-K
465 CBD could be reversed by the presence of VirD2/T-strands, we infected roots with a *virE2*
466 mutant *Agrobacterium* strain harboring a T-DNA with a mCherry-intron-NLS expression
467 cassette (At2405). Time-lapse confocal microscopy still indicated no movement of VirE2-Venus
468 in the mCherry expressing cells. (Table 1 and Supplemental Figure S19).
469 Taken together, our results indicate that myosin XI-K but not myosin VIII proteins are
470 important for VirE2 intracellular trafficking. We suggest that myosin VIII proteins help tether

471 VirE2 to the plasma membrane/peripheral regions of the cell. Upon introduction of VirD2/T-
472 strands, VirE2 is released and is trafficked through the cell by myosin XI-K.
473
474 **VirE2 delivered from *Agrobacterium* into plant cells moves along filaments**
475 The experiments conducted above measured VirE2 movement when the protein was
476 expressed *in planta*. To determine if VirE2 movement also occurred when the protein is
477 delivered from *Agrobacterium*, we adapted the split GFP system of Li and Pan (2017). We
478 internally tagged VirE2 with GFP11 and used an *Agrobacterium* strain harboring this construct
479 to infiltrate leaves of *Arabidopsis* expressing GFP1-10. Such an internally tagged VirE2 protein
480 is active in transformation (Li and Pan, 2017). Forty eight hr post infiltration, we imaged the
481 leaves using confocal microscopy. As a control, we imaged the leaves of uninfected GFP1-10
482 *Arabidopsis* plants. Similar to what we saw when VirE2-Venus was made in *Arabidopsis* root
483 cells, VirE2 introduced into plant cells from *Agrobacterium* localized in the cytoplasm
484 predominantly at the cellular periphery, but also along filaments traversing the cell (Figure 13).
485 Time-lapse confocal microscopy of 19 VirE2 aggregates indicated that they moved along these
486 filaments with a velocity of 0.323 ± 0.08 μm/sec, similar to that of VirE2-Venus made *in planta*
487 (Table 1).
488

489 # DISCUSSION
490

491 **Importance of VirE2 in *Agrobacterium*-mediated plant transformation**

492 *Agrobacterium tumefaciens* can transfer virulence (Vir) proteins and T-DNA into plant, fungal,
493 and yeast cells (Chilton et al., 1977; Bundock et al., 1995; Piers et al., 1996; de Groot et al.,
494 1998). During the transfer process, VirE2, the most abundant virulence protein (Engstrom et al.,
495 1987), and four other Vir proteins exit the bacterium via a VirB/VirD4 type IV secretion system
496 (T4SS) and facilitate transformation (Schrammeijer et al., 2003; Cascales and Christie, 2004;
497 Vergunst et al., 2005). VirE2 is a single-strand (ss) DNA binding protein that binds ssDNA *in*
498 *vitro* (Zupan et al., 1996). A popular theory proposes that VirE2 binds T-strands that enter the
499 plant cell following infection by *Agrobacterium*, and that the resulting hypothetical T-
500 complexes, composed of VirD2 covalently linked to T-strands and coated by VirE2 molecules,
501 are the form of T-DNA that traffics within the cell (Li et al., 2020). However, T-complexes have
502 not yet been identified in *Agrobacterium*-infected plants.

503 *virE2* mutant *Agrobacterium* strains are highly attenuated in virulence (Stachel and Nester,
504 1986). Fewer T-strands can be isolated from plant cells infected by an *Agrobacterium virE2*
505 mutant than from cells infected by a wild-type *Agrobacterium* strain (Yusibov et al., 1994), and
506 the few transformants produced by a *virE2* mutant *Agrobacterium* strain generally harbor large
507 T-DNA deletions, suggesting a protective function of VirE2 on T-strands (Rossi et al., 1996).
508 However, a *virE2* mutant *Agrobacterium* strain can efficiently transform plants expressing VirE2
509 (*in planta* complementation), indicating both the importance of VirE2 in transformation and that
510 the function of VirE2 in transformation occurs within the plant (Citovsky et al., 1992; Lapham et
511 al., 2021). The efficient rescue of an *Agrobacterium virE2* mutant by *in planta* complementation
512 suggests that VirE2 trafficking within a plant cell can be studied using plant lines that produce
513 VirE2. This is corroborated by our finding that active VirE2-iGFP11, when transferred from
514 *Agrobacterium*, localizes predominantly to the leaf cell periphery (Figure 13), similar to what we
515 observe with *in planta*-synthesized VirE2. In addition, movement of *Agrobacterium*-delivered
516 VirE2 along cytoplasmic filaments occurs with the same velocity as does *in planta*-made VirE2-
517 Venus (Table 1). Taken together, these findings validate our cytological observations of VirE2
518 localization and interaction with myosin proteins using *in planta*-made VirE2.

519 As well as its proposed protective function, VirE2 may facilitate T-DNA entry into the plant
520 by forming single-strand DNA-specific pores in the plant plasma membrane, as it can in artificial
521 membranes (Dumas et al., 2001). Following transfer to the plant, VirE2 initially accumulates on
522 the cytoplasmic side of host plasma membranes at points where bacteria contact the plant cell (Li
523 and Pan, 2017). Accumulation of VirE2 on the membrane is facilitated by its interaction with
524 the *Agrobacterium* effector protein VirE3, which also accumulates in the host plasma membrane
525 at contact sites with the bacteria (Lacroix et al., 2005; Li et al., 2018; Li et al., 2020). Interaction
526 of VirE2 with importin alpha may help guide VirE2 towards the nucleus (Bhattacharjee et al.,
527 2008), although this interaction is weak (Chang et al., 2014). Therefore, VirE2 may be involved
528 in the trafficking of the T-complex inside the plant cell. However, our knowledge of the precise
529 trafficking process of VirE2 inside the host cells, and the proteins that coordinate this trafficking
530 to facilitate transformation, remains sparse.
531
532 **Importance of the actin cytoskeleton for transformation and intracellular VirE2 movement**
533 The actin cytoskeleton is essential for numerous biological processes in plants, including cell
534 morphogenesis, tip growth, organelle movement, vesicle trafficking, and maintenance of cell
535 polarity ((Hussey et al., 2006; Staiger et al., 2009; Duan and Tominaga, 2018). Actin genes are
536 categorized according to their expression patterns. In *Arabidopsis*, the vegetative actins (*ACT2*,
537 *ACT7*, and *ACT8*) are mainly expressed in roots (Meagher et al., 1999), whereas *ACT4* and
538 *ACT12* are primarily expressed during pollen development (Huang et al., 1996). We conducted
539 transient and stable root transformation assays of *act2* and *act7* mutants (Figure 1A). These
540 assays indicated that mutation of these genes greatly inhibited root transformation. Restoration
541 of transformation-susceptibility by introducing an *ACT7* cDNA into *act7* mutant plants
542 confirmed that the transformation deficiency of the *act7* mutant was caused by mutation of this
543 gene. Mutation of the pollen-expressed *ACT12* gene had no effect on root transformation, as
544 expected. In addition, we measured the velocity of VirE2-Venus movement along actin
545 filaments, which were marked with mCherry-ABD2, in *Arabidopsis* cells. VirE2 aggregates
546 moved with an average velocity of 0.353 ± 0.06 μm/sec in leaf cells and 0.312 ± 0.07 μm/sec in
547 root cells (Table 1), similar to the velocity (0.434 μm/sec) recorded by Yang et al. (2017) within
548 tobacco leaf cells.

549 Salman et al. (2005) showed that VirE2 binds to microtubules *in vitro*, and Sakalis et al.,
550 (2014) showed colocalization of YFP-VirE2 with fluorescently tagged microtubules in yeast and
551 plant cells. However, they did not assay transformation in the presence of microtubule
552 disrupting agents. We observed no difference in transformation between wild-type and *bot-1*
553 mutant *Arabidopsis* roots, which have a disorganized cortical microtubule network, indicating
554 that correctly organized microtubules are not required for efficient transformation of plants.
555

556 **Importance of *Arabidopsis* myosin isoforms for transformation**

557 The movement of molecules, vesicles, and organelles along actin filaments relies on the highly
558 conserved myosin motors (Avisar et al., 2008b; Madison and Nebenfuhr, 2013; Ueda et al.,
559 2015; Citovsky and Liu, 2017). Myosins have actin-binding, ATPase, and cargo binding
560 domains, and these activities contribute to a wide range of physiological processes, including
561 root hair growth, organelle motility, tip growth of pollen tubes, and gamete nuclear migration
562 (Prokhnevsky et al., 2008; Peremyslov et al., 2010; Kawashima and Tachikawa, 2014; Madison
563 et al., 2015). *Arabidopsis* contains two classes of myosins, the plant-specific myosin VIII class
564 comprising four members (myosins VIII-1, 2, A, and B) and the myosin XI class comprising 13
565 members (myosins XI-A through K, and myosins XI-1 and XI-2). Most of the myosin XI
566 proteins are localized in the cytosol and are responsible for intracellular movement of their
567 cargos, including vesicles and organelles (Peremyslov et al., 2008; Peremyslov et al., 2010).
568 Myosin XI-K in particular is important for vesicular trafficking (Yang et al., 2014). Myosin VIII
569 proteins localize predominantly to the cellular periphery, including the plasma membrane,
570 plasmodesmata, and cortical microtubules (Golomb et al., 2008; Haraguchi et al., 2014; Bar-
571 Sinai et al., 2022) although we have found that myosin VIII-2 also localizes to the nucleus
572 (Figure 9). Myosin VIII proteins may be important for intercellular movement of viral proteins
573 and for helping guide plant cell division (Avisar et al., 2008a; Amari et al., 2014; Wu and
574 Bezanilla, 2014).
575 Upon entry into a plant cell, VirE2 may interact with VirE3 and associate with the plasma
576 membrane where myosin VIII proteins localize, then move towards the nucleus after associating
577 with T-DNA (Tu et al., 2018). We therefore tested the importance of each myosin XI and
578 myosin VIII protein for transformation by conducting transient and stable root transformation
579 assays on individual myosin gene mutants (Figures 1B and 1C). Interestingly, only disruption of

580 the myosin *XI-h* gene substantially (greater than two-fold) inhibited transformation
581 (Supplemental Figure S1A). Myosin XI-H is moderately strongly expressed in all root tissues
582 and is phylogenetically most closely related to myosins XI-B and XI-G, that are not well-
583 expressed in roots, and to myosin XI-2 which does show root expression (Peremyslov et al.,
584 2011). No specific cellular function had previously been assigned to myosin XI-H (reviewed by
585 Duan and Tominaga, 2018). We were somewhat surprised not to see an effect of a myosin *xi-k*
586 mutation on transformation because Yang et al. (2017) showed that RNAi inhibition of *N.*
587 *benthamiana* myosin XI-K decreased *Agrobacterium*-mediated transformation by ~50%.
588 However, *Arabidopsis* may encode more myosin XI isoforms than does *N. benthamiana* (Avisar
589 et al., 2008b), permitting functional redundancy of the *Arabidopsis* myosin XI isoforms to
590 conceal a role for *Arabidopsis* myosin XI-K in transformation.
591 Because the vast majority of single myosin XI or myosin VIII mutants did not affect
592 transformation, we tested the effect of higher order myosin mutants on this process. Roots from
593 plants mutant in two, three, or four myosin XI genes showed increasing deficiency in
594 transformation susceptibility (Figures 1B and 1C). As previously noted, these higher order
595 myosin XI mutants showed increasing root developmental defects as more myosin XI genes
596 were mutated (Supplemental Figure S1B; Ojangu et al., 2007; Peremyslov et al., 2008). Because
597 our *Arabidopsis* transformation assays were conducted on roots, the natural target for
598 *Agrobacterium*-mediated transformation, we were concerned that these root developmental
599 problems may complicate the interpretation of our transformation data. We therefore turned our
600 attention to higher order *Arabidopsis* myosin VIII mutants whose roots appeared normal
601 (Supplemental Figure S1B). These higher order myosin VIII mutants also showed decreased
602 transformation susceptibility (Figures 1B and 1C).
603 To test the importance of each myosin *VIII* gene in transformation, we individually expressed
604 cDNAs for each of the myosin VIII proteins in the myosin *VIII-1/2/a/b* quadruple mutant. Three
605 of these genes, encoding myosins VIII-2, A, and B, could partially restore transformation
606 susceptibility to the quadruple mutant (Figure 2A), indicating that they play an important role in
607 transformation. Simultaneous expression of pairs of these cDNAs in the quadruple mutant
608 further increased transformation (Figure 2C), indicating that these myosin VIII proteins are not
609 completely redundant with regard to transformation. However, expression of the cDNA
610 encoding myosin VIII-1 did not affect transformation (Figure 2A), suggesting a fundamental

611 difference among these class VIII myosins for their roles in *Agrobacterium*-mediated
612 transformation. As shown in Figures 6, 7, 8, 10 and discussed below, myosins VIII-2, VIII-A,
613 and VIII-B can directly interact with *Agrobacterium* VirE2, an important effector protein for
614 transformation, whereas myosin VIII-1 does not directly interact with VirE2. However, it may
615 indirectly interact with VirE2 within a protein complex. Ectopically expressed myosin VIII-A,
616 VIII-B, VIII-1, and VIII-2 localize strongly to the peripheral regions of root cells (myosin VIII-2
617 also localizes in the nucleus). Furthermore, expression of the CBDs of myosins VIII-2 and VIII-
618 A decreased the size of VirE2 aggregates that form in the myosin *VIII-1/2/a/b* quadruple mutant,
619 whereas expression of the myosin VIII-1 CBD did not. These observations indicate a
620 fundamental difference among these myosin VIII isoforms in their interaction with VirE2, their
621 subcellular localization, and their effects on transformation. Interestingly, overexpression of a
622 myosin *VIII-1* cDNA in wild-type *Arabidopsis* increased transformation, indicating both that
623 myosin VIII-1 does play some role in transformation, and that this protein is limiting in wild-
624 type roots (Figure 2B). Overexpression of myosin *VIII-A*, *VIII-B*, or *VIII-2* cDNAs in wild-type
625 roots, either individually or in combination, did not alter transformation susceptibility, indicating
626 that these proteins are naturally found in amounts maximal for transformation.
627
628 **Some myosin VIII isoforms may tether VirE2 to the plasma membrane until T-strands**
629 **enter the plant cell**
630 Several studies have indicated that myosin VIII proteins, or their globular tail domains, localize
631 at the plasma membrane, especially at plasmodesmata (Radford and White, 1998; Reichelt et al.,
632 1999; Avisar et al., 2008a; Golomb et al., 2008; Amari et al., 2014). Our results showed that
633 VirE2-Venus substantially co-localizes with each of the four transgenically expressed myosin
634 VIII proteins and their CBDs at the plasma membrane of root cells, although co-localization with
635 myosin VIII-1 is less extensive (Figure 9 and Supplemental Figures S9 and S10). When roots of
636 these transgenic plants were incubated with *Agrobacterium* lacking T-DNA, the association of
637 VirE2 with the peripheral regions of the cell remained largely unchanged. However, incubation
638 of these roots with *Agrobacterium* containing T-DNA relocalized much of the VirE2-Venus
639 signal to the cytosol. In addition, incubation of roots expressing VirE2-Venus (but not any
640 myosin VIII CBD) with *Agrobacterium* containing T-DNA relocalized a portion of the VirE2-
641 Venus signal to the perinuclear area, but not into the nucleus. These results are consistent with

642 previous observations that VirE2 localizes mainly within the cytosol and, especially, perinuclear
643 regions upon infection of cells with an *Agrobacterium* strain that can transfer VirD2/T-strands to
644 plant cells, and that only a very small quantity may enter the nucleus (Li et al., 2020).
645 To examine how various myosin isoforms may faciltate VirE2 movement from the plasma
646 membrane region to the cytosol, we measured the velocity of VirE2-Venus movement along
647 mCherry-ABD2-labeled actin filaments with and without expression of various myosin VIII or
648 myosin XI-K CBDs. For these experiments, it was assumed that the CBDs could act as domiant
649 negative molecules to bind VirE2, thereby inhibiting VirE2 movement along these actin
650 filaments. VirE2 introduced from *Agrobacterium* into *Arabidopsis* leaf cells moved along
651 filaments with a velocity of 0.323 μm/sec (Table 1). In both the absence and presence of myosin
652 VIII CBD expression, VirE2 trafficked along *Arabidopsis* actin filaments with a velocity of 0.31-
653 0.40 μm/sec (Table 1), a velocity similar (~0.502 μm/sec) to that calculated by Yang et al.
654 (2017) in tobacco leaves. These data indicate that myosin VIII proteins are not important for
655 intracellular VirE2 trafficking. However, co-expression of the myosin XI-K CBD with VirE2-
656 Venus completely blocked VirE2 movement along actin filaments, suggesting that this myosin
657 isoform is at least partially responsible for intracellular VirE2 trafficking, as suggested by Yang
658 et al. (2017).
659
660 **A model for the role of myosin proteins in VirE2 plasma membrane tethering and**
661 **movement through plant cells**
662 Research from several laboratories, and this study, has informed our revised model for how
663 *Agrobacterium* virulence effector proteins, such as VirE2, and T-DNA enter a plant cell, form
664 complexes, and traffic T-DNA to the nucleus (Figure 14). VirE2 has the ability to generate pores
665 in artificial lipid membranes through which single-strand DNA molecules, such as T-strands,
666 may penetrate (Dumas et al., 2001; Duckely et al., 2005; Grange et al., 2008). VirE2 delivered
667 from *Agrobacterium* localizes to the cytoplasmic side of the plant plasma membrane, held there
668 by interaction with another virulence effector protein, VirE3 (Li et al., 2018; Li et al., 2020).
669 Our data similarly show that both *Agrobacterium*-expressed VirE2 and plant-expressed VirE2-
670 Venus, which can effect transformation by a *virE2* mutant *Agrobacterium* cell, partially localize
671 to the cytoplasmic side of the plasma membrane. We propose that VirE2 is tethered to the
672 plasma membrane by various myosin VIII isoforms. Upon entry of VirD2/T-strands into the

673 plant, VirE2 is released from the plasma membrane and associates with T-strands. This
674 hypothetical T-complex is trafficked along an actin/endoplasmic reticulum network (Yang et al.,
675 2017) by myosin XI-K, or a functionally similar myosin XI protein, towards the nucleus.
676 Consistent with this mechanism of trafficking, we have previously shown that a Rab GTPase,
677 which modulates vesicle trafficking in biosynthetic and endocytic pathways, is important for
678 transformation (Hwang and Gelvin, 2004), and that a VAP33-like SNARE protein, that localizes
679 to ER-plasma membrane contact sites (Wang et al., 2014; Wang et al., 2015), interacts with
680 VirE2 (Lee et al., 2008).
681 We are aware that one aspect of our analysis does not easily fit this proposed model:
682 Expression of the myosin XI-K CBD completely inhibited detectable VirE2 movement through
683 the cytosol but had no effect on *Agrobacterium*-mediated transformation. Inhibition of VirE2
684 movement by the myosin XI-K CBD occurred regardless of whether *Agrobacterium* was present
685 to transfer T-DNA into the cells. We note that the requirement for VirE2 in *Agrobacterium*-
686 mediated transformation is not absolute: 1. *Agrobacterium*-mediated yeast transformation does
687 not require VirE2, although mutation of *virE2* results in a ~10-fold decrease in yeast
688 transformation (Bundock et al., 1995), and 2. Some *A. rhizogenes* strains do not encode VirE2,
689 although they are highly virulent. These strains encode two proteins, GALLS-FL and GALLS-
690 CT, that can functionally complement a *virE2*-mutant *A. tumefaciens* strain, although the amino
691 acid sequence and protein domains of VirE2 and GALLS proteins are highly dissimilar (Hodges
692 et al., 2004, 2006; Ream, 2009). With regard to the results of experiments conducted in this
693 study, we suggest either that a small, undetectable population of VirE2 molecules associates with
694 incoming T-strands and traffics towards the nucleus to effect transformation, or (a somewhat
695 heretical model) that VirE2 does not interact with T-strands in plant cells and that tracking VirE2
696 movement through the cell does not correlate with intracellular T-DNA movement. Future
697 experiments will attempt to resolve this conundrum.
698

699 ## MATERIALS AND METHODS

700 **Plant and bacterial materials and growth conditions.** Seeds of wild-type (ecotype Col-0),
701 mutant, and transgenic *Arabidopsis thaliana* were surface-sterilized with 50% bleach and 0.01%
702 SDS, washed five times with sterile water, then placed on Gamborg's B5 medium (Gibco) with
703 the appropriate antibiotics (when used, hygromycin 10 μg/mL). Seedlings were grown in 16 hr
704 light/8 hr dark conditions at 25°C. *E. coli* strains were grown at 37°C in LB medium (per liter:
705 Tryptone 10 g, NaCl 10 g, Yeast extract 5 g). *A. tumefaciens* strains were grown at 28°C in YEP
706 medium (per liter: Bacto peptone 10 g, Yeast extract 10 g, NaCl 5 g). When used, antibiotic
707 concentrations were: For *E. coli*, ampicillin, 100 μg/ml; kanamycin, 50 μg/ml; spectinomycin,
708 100 μg/ml; for *A. tumefaciens*, rifampicin, 10 μg/ml; spectinomycin, 100 μg/ml. All bacterial
709 strains and plasmid constructs used in this study are listed in Supplemental Tables S1 and S2.
710
711 **Construction of plasmids and binary vectors and generation of transgenic plants.** A
712 description of all plasmids used in this study, including details of their construction, is given in
713 Supplemental Table S1. Primers used for these constructions are given in Supplemental Table
714 S3. Final *E. coli* and *A. tumefaciens* strains are given in Supplemental Table S2. Recombinant
715 constructions were transformed into *E. coli* TOP10 or DH10B before characterization and
716 transfer to the appropriate *Agrobacterium* strains by electroporation. For protein expression,
717 plasmids were transferred to *E. coli* BL21DE3. T-DNA binary vectors in *Agrobacterium* were
718 used to transform plants of the Col-0 or the *myosin VIII-1/2/a/b* quadruple mutant background
719 utilizing a floral dip transformation protocol (Clough and Bent, 1998).
720
721 ***Agrobacterium*-mediated transient and stable transformation assays.** Overnight
722 *Agrobacterium* cultures were diluted 1:10 into 20 ml of YEP medium containing the appropriate
723 antibiotics and grown at 28°C until they reached an A_{600} = 0.83 (~10^9 cells/ml). The cells were
724 collected by centrifugation, washed with sterile 0.9% NaCl, and serially diluted in 0.9% NaCl for
725 transient and stable root transformation assays. For transient transformation assays, infection of
726 *Arabidopsis* root segments was performed with *Agrobacterium* strains containing the T-DNA
727 binary vector pBISN1 (Narasimhulu et al., 1996) as previously described (Tenea et al., 2009).
728 Transformation efficiency was reported as the percentage of root segments stained blue with 5-

729 bromo-4-chloro-3-indolyl-β-D-glucuronic acid (X-gluc) after two days co-cultivation with
730 bacteria on MS medium plus an additional four days on CIM (Callus-Inducing Medium)
731 containing 100 µg/ml timentin. For stable transformation, after two days of cocultivation, root
732 segments were separated onto CIM containing 100 µg/ml timentin and the appropriate selection
733 agent. The plates were incubated at 23°C for four weeks, after which they were scored for callus
734 development on the ends of the roots. Stable transformation efficiency was calculated as the
735 percentage of total segments showing calli. Transient and stable transformation assays were
736 conducted in triplicate, with >100 root segments per replicate.
737
738 **Bimolecular fluorescence complementation (BiFC).** A VirE2 coding sequence was fused with
739 cEYFP (C-terminal 64 amino acid residues of an *EYFP* gene) and under the control of a β-
740 estradiol-inducer promoter in the vector pSAT1 to make pSAT1-Pi-VirE2-cEYFP. cDNAs
741 encoding myosin VIII CBDs were amplified using the appropriate primers (Supplemental Table
742 S3), fused with nVenus (N-terminal 174 amino acids of a *Venus* gene) and cloned, under the
743 control of a β-estradiol-inducer promoter in pSAT6, to make pSAT6-Pi-nVenus-myosin VIII
744 CBD. The Pi-VirE2-cEYFP expression cassette and the Pi-nVenus-myosin VIII CBD
745 expression cassettes were digested with *Asc*I and PI-*Psp*I, respectively, and cloned into the same
746 sites in the binary vector pE4437. pE4437 also contains a *hptII* plant selection marker, an
747 expression cassette for a nuclear marker (P_{35S}-Cerulean-NLS), and an actin cytoskeleton marker
748 (P_{35S}-mCherry-actin binding domain2, ABD2). These final constructs were introduced into *A.*
749 *tumefaciens* GV3101::pMP90 (Koncz and Schell, 1986) by electroporation to make *A.*
750 *tumefaciens* At2320-At2324, respectively, and used to generate transgenic Col-0 *Arabidopsis*
751 plants for *in vivo* BiFC assays.
752
753 **Yeast two hybrid assay**. An octopine-type VirE2 gene from pTiA6 was cloned into the bait
754 vector pGBKT7, and the myosin VIII and myosin XI CBD cDNAs were individually cloned into
755 the prey vector pGADT7 (Clontech). As negative controls, empty bait, empty prey, and Lamin
756 C prey plasmids were used (Krendel et al., 2007). A cDNA encoding the VirE2-interacting
757 protein 1 (VIP1) was used as a positive control (Tzfira et al., 2001). Yeast transformations were
758 performed using a lithium acetate method (Sato et al., 1994). Cells were plated onto synthetic

759 dropout (SD)-agar plates lacking tryptophan and leucine. Three days after transformation, yeast
760 cells from the resulting colonies were plated onto SD medium lacking tryptophan, leucine, and
761 histidine (-Trp-Leu-His) supplemented with 3-amino-1,2,4-triazole (3AT) to test for protein
762 interactions.
763
764 ***In vitro* protein pull-down assay.** The plasmid pET28a (Novagen, San Diego, CA) was used to
765 generate recombinant proteins fused in-frame with a Venus tag or a myc tag. A full-length
766 cDNA encoding VirE2 fused with Venus was cloned into pET28a with *Nco*I+*Not*I. cDNAs
767 encoding the CBDs (amino acids 953-1,166 for myosin VIII-1; amino acids 1,003-1,220 for
768 myosin VIII-2; amino acids 948-1,153 for myosin VIII-A; amino acids 954-1,136 for myosin
769 VIII-B; amino acids 808-1,531 for myosin XI-K) of myosin VIII and XI-K were amplified and
770 cloned into pET28a with *Nco*I+*Bam*HI (myosin VIII CBDs) or *Nco*I+*Not*I (myosin XI-K CBD)
771 to generate myc fusions. The full-length cDNA of VIP1 was cloned into pET28a with
772 *Nco*I+*Bam*HI to use as a myc-tagged positive control, and for negative controls Lamin C fused
773 with a myc tag, or Venus only, were cloned into pET28a with *Sma*I+*Bam*HI. The constructs
774 were transformed into *E. coli* BL21 (DE3). Bacteria were cultured at 16°C for 18 hours in the
775 presence of 0.5 mM isopropylthio-β-galactoside (IPTG). The cells were centrifuged and the
776 pellet was sonicated in cell lysis buffers (20 mM HEPES-KOH pH 7.2, 50 mM potassium
777 acetate, 50 mM KCl, 1 mM EDTA, 1 mM EGTA, 1 mM DTT, 5% glycerol, 0.5% Triton X-100,
778 1 mM phenylmethylsulfonylfluoride [PMSF]). VirE2-Venus and Venus cell lysates were
779 incubated with GFP-Trap magnetic agarose beads (Chromotek, USA) at 4°C for 2 hr with gentle
780 shaking. The beads were washed three times with cell lysate buffer (0.2% Triton X-100) and
781 then incubated with bacterial lysates from *E. coli* cells expressing myc-tagged VIP1, myc-tagged
782 Lamin C, or myc-tagged myosin VIII/XI-K CBDs proteins that were prepared as described
783 above. The binding reactions were incubated at 4°C for 1 hr with gentle shaking. The beads
784 were washed three times with cell lysate buffer (0.2% Triton X-100) followed by boiling in
785 sodium dodecyl sulfate polyacrylamide gel electrophoresis (SDS-PAGE) buffer for 10 min.
786 Protein samples were loaded onto 10% SDS polyacrylamide gels, subjected to electrophoresis
787 (60 Volts 1.5 hrs for the stacking gel and 100 Volts 4.5 hrs for the separating gel), then either
788 stained with Coomassie blue or subjected to western blot analysis using a 1:1000 dilution of
789 mouse anti-GFP or mouse anti-Myc antibodies (Cell Signaling Technology, USA). After

790 addition of a 1:5000 dilution of horseradish peroxidase-conjugated horse anti-mouse secondary
791 antibodies (Catalog #7076; Cell Signaling Technology, USA), proteins were detected using an
792 ECL kit (LI-COR Biosciences, Lincoln, NE, USA).
793
794 ***In vivo* co-immunoprecipitation (co-IP) assay.** Transgenic *Arabidopsis* plants (generated using
795 *Agrobacterium* strains At2423-At2427) harboring an inducible expression cassette of either
796 VirE2-Venus, or Venus, and of each myc-tagged myosin VIII or XI-K CBDs were used for *in*
797 *vivo* protein-protein interaction assays. Transgenic lines expressing, upon induction, myc-tagged
798 CBDs and Venus were used as negative controls (At2428). Four-week old plants were treated
799 with 5 μM β-estradiol for 24 hr, and roots were harvested and ground in liquid nitrogen using a
800 mortar and pestle. A total of 0.25 g of the ground tissue was transferred into a 2 ml tube and 500
801 μl of CoIP buffer (50 mM Tris-HCl, pH 7.5, 150 mM NaCl, 0.1% Triton X-100, 0.2% Nonidet
802 P-40, 0.6 mM PMSF, and 20 μM MG132 in a Roche protease inhibitor cocktail) was added. The
803 mixture was mixed thoroughly by repeated cycles of 30 sec vortexing followed by chilling on
804 ice. The samples were centrifuged at 4°C, 13000g for 5 min. A total of 20 μl of anti-GFP beads
805 was pre-washed with wash buffer (50 mM Tris-HCl, pH 7.5, 150 mM NaCl, 0.6 mM PMSF, and
806 20 μM MG132 with Roche protease inhibitor cocktail) three times, the beads were added to the
807 extracted supernatant solution, and the reactions were incubated at 4°C for 1 hr with gentle
808 shaking. The beads were washed five times with wash buffer, proteins were eluted by incubation
809 with 4x LDS sample loading buffer (Invitrogen, CA, USA) at 95℃ for 3 min. The proteins were
810 fractionated by SDS-PAGE and analyzed using western blots, with a 1:1000 dilution of anti-GFP
811 and anti-Myc antibodies, respectively. The proteins were detected using an ECL kit (LI-COR
812 Bioscienccs, Lincoln, NE, USA).
813
814 **Localization of VirE2-Venus after infection of *Arabidopsis* roots with *Agrobacterium* strains**
815 **harboring or lacking T-DNA.** Transgenic *A. thaliana* lines expressing a *VirE2-Venus* gene
816 under the control of a β-estradiol inducible promoter were treated with 5 μM β-estradiol for 24
817 hr. Roots were infected with a *virE2* mutant strain *A. tumefaciens* strain (*A. tumefaciens*
818 EHA105 containing a non-polar deletion of *virE2*; At1872) containing the plasmid pBBR1-
819 MCS2::mCherry to track red fluorescent bacteria (At2405). The *Agrobacterium* cells either
820 contained or lacked the T-DNA binary vector pE4672 (*A. tumefaciens* At2404 and At2403,

821 respectively). Overnight bacterial cultures were transferred to fresh AB-glucose medium and
822 grown until the cell density reached an A_{600}=0.83. The bacteria were centrifuged and
823 resuspended in induction medium (1x AB salts, 2% glucose, 30 mM MES, 2 mM Na_2HPO4, 2
824 mM NaH_2PO4) containing 100 μM acetosyringone and cultured for 16-20 hr. Six hr after
825 cocultivation with bacteria at 10^8 cfu/ml, root segments were observed by confocal microscopy
826 (Zesis 880 Upright Confocal microscope with a Plan-Apo 20×/0.8 objective). Images from 100
827 cells of each infection were analyzed using Image J.
828
829 **Localization of VirE2-Venus after infiltration of *Arabidopsis* GFP1-10 leaves with an**
830 ***Agrobacterium* strain expressing VirE2-iGFP11.**
831
832 The delivery of *Agrobacterium*-derived VirE2 to *Arabidopsis* was performed by a split-GFP
833 approach as described previously (Li et al., 2014). Briefly, the large fragment GFP1-10 was
834 expressed in transgenic *Arabidopsis* plants. A plasmid encoding the small GFP11 fragment
835 fused internally with VirE2 was introduced into *A. tumefaciens* At1872 (lacking *virE2*) and used
836 to infiltrate *Arabidopsis* leaves expressing GFP1-10. GFP fluorescence signals were visualized
837 by confocal microscopy. For Agro-infiltration, *Agrobacteria* expressing VirE2-GFP11 was
838 cultured in YEP medium supplied with spectinomycin at 28°C overnight until they reached an
839 A_{600}= 0.8. The bacteria were collected by centrifugation and the pellet was washed in infiltration
840 solution (10 mM MES, pH 5.6, 10 mM $MgCl_2$, 200 μM acetosyringone). The bacterial cells
841 were suspended in infiltration solution to an A_{600}= 0.8-1. The bacteria were maintained at room
842 temperature for 2-4 hours, then infiltrated into *Arabidopsis* leaves using a 1 mL syringe.
843 Infiltrated plants were maintained in the dark overnight, then transferred to an illuminated
844 growth chamber until imaging.
845
846 **Confocal microscopy imaging.** For VirE2-Venus trafficking, transgenic plantlets harboring an
847 inducible *Venus-VirE2* transgene (generated using *A. tumefaciens* At2365-At2369) were placed
848 on B5 agar plates containing 100 μg/ml timentin and 20 μg/ml hygromycin and grown vertically
849 for one week. The plants were treated with 10 μM β-estradiol for 9 hr, washed with sterile
850 water, and time lapse images of the roots were taken using a Zeiss 880 confocal microscope

851 equipped with a 20 X water objective. For VirE2 relocalization assays, similarly grown plants
852 were treated with 5 μM β-estradiol for 24 hr, washed with sterile water, and infected with 10^8
853 cfu/ml of a *virE2* mutant *Agrobacterium* strain containing or lacking a T-DNA binary vector.
854 Infections were conducted for 8 hr as described above, and images were taken using a Zeiss 880
855 confocal microscope equipped with a Plan-Apo 20×/0.8 objective.
856

857 **SUPPLEMENTAL DATA**

858 **Supplemental Figure S1.** Most *myosin VIII* and *myosin XI* single mutants are not deficient in
859 stable transformation.
860 **Supplemental Figure S2.** Growth and morphology of wild-type and higher order *myosin VIII*
861 and *XI* mutant plants.
862 **Supplemental Figure S3.** Effect on transformation of expressing full-length myosin cDNAs in
863 wild-type and *myosin VIII-1/2/a/b* mutant plants.
864 **Supplemental Figure S4.** Effect on transformation of expressing full-length inducible myosin
865 cDNAs in wild-type and *myosin VIII-1/2/a/b* mutant plants.
866 **Supplemental Figure S5.** Effect on transformation of expressing pairs of full-length myosin
867 cDNAs in wild-type and *myosin VIII-1/2/a/b* mutant plants.
868 **Supplemental Figure S6.** Inducible expression of myosin VIII, but not myosin XI-K, CBDs
869 inhibits transformation.
870 **Supplemental Figure S7.** Co-localization of VirE2-Venus and FM4-64.
871 **Supplemental Figure S8.** Subcellular localization of VirE2-Venus in transgenic plants.
872 **Supplemental Figure S9.** Myosin VIII CBDs colocalize with the plasma membrane marker
873 PIP2A.
874 **Supplemental Figure S10.** VirE2 re-localizes to the perinuclear area after infection by an
875 *Agrobacterium* strain that can transfer T-DNA.
876 **Supplemental Figure S11.** Infection of root cells with an *Agrobacterium* strain capable of
877 transferring T-DNA re-localizes VirE2-Venus from the cellular periphery into the cytoplasm.
878 **Supplemental Figure S12.** Infection of root cells with an *Agrobacterium* strain capable of
879 transferring T-DNA does not re-localizes VirE2-Venus from the cellular periphery into the
880 cytoplasm when the myosin VIII-1 CBD is expressed.

881 **Supplemental Figure S13.** Infection of root cells with an *Agrobacterium* strain capable of
882 transferring T-DNA re-localizes VirE2-Venus from the cellular periphery into the cytoplasm.
883 **Supplemental Figure S14.** Infection of root cells with an *Agrobacterium* strain capable of
884 transferring T-DNA re-localizes VirE2-Venus from the cellular periphery into the cytoplasm.
885 **Supplemental Figure S15.** Infection of root cells with an *Agrobacterium* strain capable of
886 transferring T-DNA re-localizes VirE2-Venus from the cellular periphery into the cytoplasm.
887 **Supplemental Figure S16.** Expression of the myosin XI-K CBD does not affect VirE2-Venus
888 localization upon infection by *Agrobacterium.*
889 **Supplemental Figure S17.** Expression of the myosin XI-K CBD inhibits movement of VirE2-
890 Venus.
891

892 ## ACKNOWLEDGEMENTS
893 The authors thank Dr. Valerian V. Dolja, Oregon State University, for providing the *Arabidopsis*
894 mutant lines. We thank the Purdue University Imaging Facility for use of their confocal
895 microscope. We also thank Dr. Kiran Mysore for critical reading of the manuscript. Dr. Praveen
896 Rao contributed data for Figure 1A. Ms. Fang-Yu Hsu contributed data for Figures 4D and 4E.
897

898 ## FUNDING
899 This project was supported by grants from the US National Science Foundation: IOS 1725122
900 and IOS-2006668. DNA sequence data were obtained with partial support from a P30 grant
901 (CA023168) to the Purdue University Cancer Center.
902
903

904 **REFERENCES**

905

906 **Amari, K., Di Donato, M., Dolja, V.V., and Heinlein, M.** (2014). Myosins VIII and XI play
907 distinct roles in reproduction and transport of tobacco mosaic virus. PLoS Pathog **10,**
908 e1004448.
909 **Avisar, D., Prokhnevsky, A.I., and Dolja, V.V.** (2008a). Class VIII myosins are required for
910 plasmodesmatal localization of a closterovirus Hsp70 homolog. J Virol **82,** 2836-2843.
911 **Avisar, D., Prokhnevsky, A.I., Makarova, K.S., Koonin, E.V., and Dolja, V.V.** (2008b).
912 Myosin XI-K Is required for rapid trafficking of Golgi stacks, peroxisomes, and
913 mitochondria in leaf cells of Nicotiana benthamiana. Plant Physiol **146,** 1098-1108.
914 **Bevan, M.W., and Chilton, M.D.** (1982). T-DNA of the Agrobacterium Ti and Ri plasmids.
915 Annu Rev Genet **16,** 357-384.
916 **Bezanilla, M., Horton, A.C., Sevener, H.C., and Quatrano, R.S.** (2003). Phylogenetic analysis
917 of new plant myosin sequences. J Mol Evol **57,** 229-239.
918 **Bhattacharjee, S., Lee, L.Y., Oltmanns, H., Cao, H., Veena, Cuperus, J., and Gelvin, S.B.**
919 (2008). IMPa-4, an Arabidopsis importin alpha isoform, is preferentially involved in
920 agrobacterium-mediated plant transformation. Plant Cell **20,** 2661-2680.
921 **Bichet, A., Desnos, T., Turner, S., Grandjean, O., and Hofte, H.** (2001). BOTERO1 is
922 required for normal orientation of cortical microtubules and anisotropic cell expansion in
923 Arabidopsis. Plant J **25,** 137-148.
924 **Bundock, P., den Dulk-Ras, A., Beijersbergen, A., and Hooykaas, P.J.** (1995). Trans-
925 kingdom T-DNA transfer from Agrobacterium tumefaciens to Saccharomyces cerevisiae.
926 EMBO J **14,** 3206-3214.
927 **Cascales, E., and Christie, P.J.** (2004). Definition of a bacterial type IV secretion pathway for a
928 DNA substrate. Science **304,** 1170-1173.
929 **Chang, C.W., Williams, S.J., Counago, R.M., and Kobe, B.** (2014). Structural basis of
930 interaction of bipartite nuclear localization signal from Agrobacterium VirD2 with rice
931 importin-alpha. Mol Plant **7,** 1061-1064.
932 **Chilton, M.D., Drummond, M.H., Merio, D.J., Sciaky, D., Montoya, A.L., Gordon, M.P.,**
933 **and Nester, E.W.** (1977). Stable incorporation of plasmid DNA into higher plant cells:
934 the molecular basis of crown gall tumorigenesis. Cell **11,** 263-271.
935 **Christie, P.J., Atmakuri, K., Krishnamoorthy, V., Jakubowski, S., and Cascales, E.** (2005).
936 Biogenesis, architecture, and function of bacterial type IV secretion systems. Annu Rev
937 Microbiol **59,** 451-485.
938 **Citovsky, V., and Liu, B.** (2017). Myosin-driven transport network in plants is functionally
939 robust and distinctive. Proc Natl Acad Sci U S A **114,** 1756-1758.
940 **Citovsky, V., Wong, M.L., and Zambryski, P.** (1989). Cooperative interaction of
941 Agrobacterium VirE2 protein with single-stranded DNA: implications for the T-DNA
942 transfer process. Proc Natl Acad Sci U S A **86,** 1193-1197.
943 **Citovsky, V., Zupan, J., Warnick, D., and Zambryski, P.** (1992). Nuclear localization of
944 Agrobacterium VirE2 protein in plant cells. Science **256,** 1802-1805.
945 **de Groot, M.J., Bundock, P., Hooykaas, P.J., and Beijersbergen, A.G.** (1998).
946 Agrobacterium tumefaciens-mediated transformation of filamentous fungi. Nat
947 Biotechnol **16,** 839-842.

948 **Djamei, A., Pitzschke, A., Nakagami, H., Rajh, I., and Hirt, H.** (2007). Trojan horse strategy
949 in Agrobacterium transformation: abusing MAPK defense signaling. Science **318,** 453-
950 456.
951 **Duan, Z., and Tominaga, M.** (2018). Actin-myosin XI: an intracellular control network in
952 plants. Biochem Biophys Res Commun **506,** 403-408.
953 **Duckely, M., Oomen, C., Axthelm, F., Van Gelder, P., Waksman, G., and Engel, A.** (2005).
954 The VirE1VirE2 complex of Agrobacterium tumefaciens interacts with single-stranded
955 DNA and forms channels. Mol Microbiol **58,** 1130-1142.
956 **Dumas, F., Duckely, M., Pelczar, P., Van Gelder, P., and Hohn, B.** (2001). An
957 Agrobacterium VirE2 channel for transferred-DNA transport into plant cells. Proc Natl
958 Acad Sci U S A **98,** 485-490.
959 **Dym, O., Albeck, S., Unger, T., Jacobovitch, J., Branzburg, A., Michael, Y., Frenkiel-**
960 **Krispin, D., Wolf, S.G., and Elbaum, M.** (2008). Crystal structure of the
961 Agrobacterium virulence complex VirE1-VirE2 reveals a flexible protein that can
962 accommodate different partners. Proc Natl Acad Sci U S A **105,** 11170-11175.
963 **Embley, T.M., and Martin, W.** (2006). Eukaryotic evolution, changes and challenges. Nature
964 **440,** 623-630.
965 **Engstrom, P., Zambryski, P., Van Montagu, M., and Stachel, S.** (1987). Characterization of
966 Agrobacterium tumefaciens virulence proteins induced by the plant factor
967 acetosyringone. J Mol Biol **197,** 635-645.
968 **Foth, B.J., Goedecke, M.C., and Soldati, D.** (2006). New insights into myosin evolution and
969 classification. Proc Natl Acad Sci U S A **103,** 3681-3686.
970 **Gelvin, S.B.** (1998). Agrobacterium VirE2 proteins can form a complex with T strands in the
971 plant cytoplasm. J Bacteriol **180,** 4300-4302.
972 **Gelvin, S.B.** (2000). Agrobacterium and Plant Genes Involved in T-DNA Transfer and
973 Integration. Annu Rev Plant Physiol Plant Mol Biol **51,** 223-256.
974 **Gelvin, S.B.** (2006). Agrobacterium transformation of Arabidopsis thaliana roots: a quantitative
975 assay. Methods Mol Biol **343,** 105-113.
976 **Gelvin, S.B.** (2010). Finding a way to the nucleus. Curr Opin Microbiol **13,** 53-58.
977 **Gelvin, S.B.** (2017). Integration of Agrobacterium T-DNA into the plant genome. Annual review
978 of genetics **51,** 22.
979 **Golomb, L., Abu-Abied, M., Belausov, E., and Sadot, E.** (2008). Different subcellular
980 localizations and functions of Arabidopsis myosin VIII. BMC Plant Biol **8,** 3.
981 **Grange, W., Duckely, M., Husale, S., Jacob, S., Engel, A., and Hegner, M.** (2008). VirE2: a
982 unique ssDNA-compacting molecular machine. PLoS Biol **6,** e44.
983 **Howard, C.A., Gummere, G.R., Lyon, M.F., Bennett, D., and Artzt, K.** (1990). Genetic and
984 molecular analysis of the proximal region of the mouse t-complex using new molecular
985 probes and partial t-haplotypes. Genetics **126,** 1103-1114.
986 **Huang, S., An, Y.Q., McDowell, J.M., McKinney, E.C., and Meagher, R.B.** (1996). The
987 Arabidopsis thaliana ACT4/ACT12 actin gene subclass is strongly expressed throughout
988 pollen development. Plant J **10,** 189-202.
989 **Hussey, P.J., Ketelaar, T., and Deeks, M.J.** (2006). Control of the actin cytoskeleton in plant
990 cell growth. Annu Rev Plant Biol **57,** 109-125.
991 **Hwang, H.H., and Gelvin, S.B.** (2004). Plant proteins that interact with VirB2, the
992 Agrobacterium tumefaciens pilin protein, mediate plant transformation. Plant Cell **16,**
993 3148-3167.

994 **Kawashima, Y., and Tachikawa, M.** (2014). Ab Initio Path Integral Molecular Dynamics Study
995 of the Nuclear Quantum Effect on Out-of-Plane Ring Deformation of Hydrogen Maleate
996 Anion. J Chem Theory Comput **10,** 153-163.
997 **Krendel, M., Osterweil, E.K., and Mooseker, M.S.** (2007). Myosin 1E interacts with
998 synaptojanin-1 and dynamin and is involved in endocytosis. FEBS Lett **581,** 644-650.
999 **Lacroix, B., Vaidya, M., Tzfira, T., and Citovsky, V.** (2005). The VirE3 protein of
1000 Agrobacterium mimics a host cell function required for plant genetic transformation.
1001 EMBO J **24,** 428-437.
1002 **Lapham, R.A., Lee, L.Y., Xhako, E., Gomez, E.G., Nivya, V.M., and Gelvin, S.B.** (2021).
1003 Agrobacterium VirE2 Protein Modulates Plant Gene Expression and Mediates
1004 Transformation From Its Location Outside the Nucleus. Front Plant Sci **12,** 684192.
1005 **Lee, L.Y., Fang, M.J., Kuang, L.Y., and Gelvin, S.B.** (2008). Vectors for multi-color
1006 bimolecular fluorescence complementation to investigate protein-protein interactions in
1007 living plant cells. Plant Methods **4,** 24.
1008 **Lee, Y.R., and Liu, B.** (2004). Cytoskeletal motors in Arabidopsis. Sixty-one kinesins and
1009 seventeen myosins. Plant Physiol **136,** 3877-3883.
1010 **Li, X., and Pan, S.Q.** (2017). Agrobacterium delivers VirE2 protein into host cells via clathrin-
1011 mediated endocytosis. Sci Adv **3,** e1601528.
1012 **Li, X., Tu, H., and Pan, S.Q.** (2018). Agrobacterium Delivers Anchorage Protein VirE3 for
1013 Companion VirE2 to Aggregate at Host Entry Sites for T-DNA Protection. Cell Rep **25,**
1014 302-311 e306.
1015 **Li, X., Yang, Q., Tu, H., Lim, Z., and Pan, S.Q.** (2014). Direct visualization of
1016 Agrobacterium-delivered VirE2 in recipient cells. Plant J **77,** 487-495.
1017 **Li, X., Yang, Q., Peng, L., Tu, H., Lee, L.Y., Gelvin, S.B., and Pan, S.Q.** (2020).
1018 Agrobacterium-delivered VirE2 interacts with host nucleoporin CG1 to facilitate the
1019 nuclear import of VirE2-coated T complex. Proc Natl Acad Sci U S A **117,** 26389-26397.
1020 **Madison, S.L., and Nebenfuhr, A.** (2013). Understanding myosin functions in plants: are we
1021 there yet? Curr Opin Plant Biol **16,** 710-717.
1022 **Madison, S.L., Buchanan, M.L., Glass, J.D., McClain, T.F., Park, E., and Nebenfuhr, A.**
1023 (2015). Class XI Myosins Move Specific Organelles in Pollen Tubes and Are Required
1024 for Normal Fertility and Pollen Tube Growth in Arabidopsis. Plant Physiol **169,** 1946-
1025 1960.
1026 **Meagher, R.B., McKinney, E.C., and Kandasamy, M.K.** (1999). Isovariant dynamics expand
1027 and buffer the responses of complex systems: the diverse plant actin gene family. Plant
1028 Cell **11,** 995-1006.
1029 **Narasimhulu, S.B., Deng, X.B., Sarria, R., and Gelvin, S.B.** (1996). Early transcription of
1030 Agrobacterium T-DNA genes in tobacco and maize. Plant Cell **8,** 873-886.
1031 **Ojangu, E.L., Jarve, K., Paves, H., and Truve, E.** (2007). Arabidopsis thaliana myosin XIK is
1032 involved in root hair as well as trichome morphogenesis on stems and leaves.
1033 Protoplasma **230,** 193-202.
1034 **Peremyslov, V.V., Prokhnevsky, A.I., and Dolja, V.V.** (2010). Class XI myosins are required
1035 for development, cell expansion, and F-Actin organization in Arabidopsis. Plant Cell **22,**
1036 1883-1897.
1037 **Peremyslov, V.V., Prokhnevsky, A.I., Avisar, D., and Dolja, V.V.** (2008). Two class XI
1038 myosins function in organelle trafficking and root hair development in Arabidopsis. Plant
1039 Physiol **146,** 1109-1116.

1040 **Peremyslov, V.V., Mockler, T.C., Filichkin, S.A., Fox, S.E., Jaiswal, P., Makarova, K.S.,**
1041 **Koonin, E.V., and Dolja, V.V.** (2011). Expression, splicing, and evolution of the myosin
1042 gene family in plants. Plant Physiol **155,** 1191-1204.
1043 **Piers, K.L., Heath, J.D., Liang, X., Stephens, K.M., and Nester, E.W.** (1996). Agrobacterium
1044 tumefaciens-mediated transformation of yeast. Proc Natl Acad Sci U S A **93,** 1613-1618.
1045 **Prokhnevsky, A.I., Peremyslov, V.V., and Dolja, V.V.** (2008). Overlapping functions of the
1046 four class XI myosins in Arabidopsis growth, root hair elongation, and organelle motility.
1047 Proc Natl Acad Sci U S A **105,** 19744-19749.
1048 **Radford, J.E., and White, R.G.** (1998). Localization of a myosin-like protein to
1049 plasmodesmata. Plant J **14,** 743-750.
1050 **Reichelt, S., Knight, A.E., Hodge, T.P., Baluska, F., Samaj, J., Volkmann, D., and**
1051 **Kendrick-Jones, J.** (1999). Characterization of the unconventional myosin VIII in plant
1052 cells and its localization at the post-cytokinetic cell wall. Plant J **19,** 555-567.
1053 **Reisen, D., and Hanson, M.R.** (2007). Association of six YFP-myosin XI-tail fusions with
1054 mobile plant cell organelles. BMC Plant Biol **7,** 6.
1055 **Richards, T.A., and Cavalier-Smith, T.** (2005). Myosin domain evolution and the primary
1056 divergence of eukaryotes. Nature **436,** 1113-1118.
1057 **Rossi, L., Hohn, B., and Tinland, B.** (1996). Integration of complete transferred DNA units is
1058 dependent on the activity of virulence E2 protein of Agrobacterium tumefaciens. Proc
1059 Natl Acad Sci U S A **93,** 126-130.
1060 **Sakalis, P.A., van Heusden, G.P., and Hooykaas, P.J.** (2014). Visualization of VirE2 protein
1061 translocation by the Agrobacterium type IV secretion system into host cells.
1062 Microbiologyopen **3,** 104-117.
1063 **Salman, H., Abu-Arish, A., Oliel, S., Loyter, A., Klafter, J., Granek, R., and Elbaum, M.**
1064 (2005). Nuclear localization signal peptides induce molecular delivery along
1065 microtubules. Biophys J **89,** 2134-2145.
1066 **Sato, T., Hanada, M., Bodrug, S., Irie, S., Iwama, N., Boise, L.H., Thompson, C.B.,**
1067 **Golemis, E., Fong, L., Wang, H.G., and et al.** (1994). Interactions among members of
1068 the Bcl-2 protein family analyzed with a yeast two-hybrid system. Proc Natl Acad Sci U
1069 S A **91,** 9238-9242.
1070 **Sattarzadeh, A., Franzen, R., and Schmelzer, E.** (2008). The Arabidopsis class VIII myosin
1071 ATM2 is involved in endocytosis. Cell Motil Cytoskeleton **65,** 457-468.
1072 **Schrammeijer, B., den Dulk-Ras, A., Vergunst, A.C., Jurado Jacome, E., and Hooykaas,**
1073 **P.J.** (2003). Analysis of Vir protein translocation from Agrobacterium tumefaciens using
1074 Saccharomyces cerevisiae as a model: evidence for transport of a novel effector protein
1075 VirE3. Nucleic Acids Res **31,** 860-868.
1076 **Sen, P., Pazour, G.J., Anderson, D., and Das, A.** (1989). Cooperative binding of
1077 Agrobacterium tumefaciens VirE2 protein to single-stranded DNA. J Bacteriol **171,**
1078 2573-2580.
1079 **Shi, Y., Lee, L.Y., and Gelvin, S.B.** (2014). Is VIP1 important for Agrobacterium-mediated
1080 transformation? Plant J **79,** 848-860.
1081 **Simone, M., McCullen, C.A., Stahl, L.E., and Binns, A.N.** (2001). The carboxy-terminus of
1082 VirE2 from Agrobacterium tumefaciens is required for its transport to host cells by the
1083 virB-encoded type IV transport system. Mol Microbiol **41,** 1283-1293.
1084 **Smith, L.G., and Oppenheimer, D.G.** (2005). Spatial control of cell expansion by the plant
1085 cytoskeleton. Annu Rev Cell Dev Biol **21,** 271-295.

1086 **Sparkes, I., Runions, J., Hawes, C., and Griffing, L.** (2009). Movement and remodeling of the
1087 endoplasmic reticulum in nondividing cells of tobacco leaves. Plant Cell **21,** 3937-3949.
1088 **Stachel, S.E., and Nester, E.W.** (1986). The genetic and transcriptional organization of the vir
1089 region of the A6 Ti plasmid of Agrobacterium tumefaciens. EMBO J **5,** 1445-1454.
1090 **Staiger, C.J., Sheahan, M.B., Khurana, P., Wang, X., McCurdy, D.W., and Blanchoin, L.**
1091 (2009). Actin filament dynamics are dominated by rapid growth and severing activity in
1092 the Arabidopsis cortical array. J Cell Biol **184,** 269-280.
1093 **Szymanski, D.B., and Cosgrove, D.J.** (2009). Dynamic coordination of cytoskeletal and cell
1094 wall systems during plant cell morphogenesis. Curr Biol **19,** R800-811.
1095 **Tenea, G.N., Spantzel, J., Lee, L.Y., Zhu, Y., Lin, K., Johnson, S.J., and Gelvin, S.B.** (2009).
1096 Overexpression of several Arabidopsis histone genes increases agrobacterium-mediated
1097 transformation and transgene expression in plants. Plant Cell **21,** 3350-3367.
1098 **Trybus, K.M.** (2008). Myosin V from head to tail. Cell Mol Life Sci **65,** 1378-1389.
1099 **Tu, H., Li, X., Yang, Q., Peng, L., and Pan, S.Q.** (2018). Real-Time Trafficking of
1100 Agrobacterium Virulence Protein VirE2 Inside Host Cells. Curr Top Microbiol Immunol
1101 **418,** 261-286.
1102 **Tzfira, T., Vaidya, M., and Citovsky, V.** (2001). VIP1, an Arabidopsis protein that interacts
1103 with Agrobacterium VirE2, is involved in VirE2 nuclear import and Agrobacterium
1104 infectivity. EMBO J **20,** 3596-3607.
1105 **Tzfira, T., Li, J., Lacroix, B., and Citovsky, V.** (2004). Agrobacterium T-DNA integration:
1106 molecules and models. Trends Genet **20,** 375-383.
1107 **Ueda, H., Tamura, K., and Hara-Nishimura, I.** (2015). Functions of plant-specific myosin XI:
1108 from intracellular motility to plant postures. Curr Opin Plant Biol **28,** 30-38.
1109 **Ueda, H., Yokota, E., Kutsuna, N., Shimada, T., Tamura, K., Shimmen, T., Hasezawa, S.,**
1110 **Dolja, V.V., and Hara-Nishimura, I.** (2010). Myosin-dependent endoplasmic reticulum
1111 motility and F-actin organization in plant cells. Proc Natl Acad Sci U S A **107,** 6894-
1112 6899.
1113 **Ueki, S., and Citovsky, V.** (2005). Identification of an interactor of cadmium ion-induced
1114 glycine-rich protein involved in regulation of callose levels in plant vasculature. Proc
1115 Natl Acad Sci U S A **102,** 12089-12094.
1116 **Vale, R.D.** (2003). The molecular motor toolbox for intracellular transport. Cell **112,** 467-480.
1117 **Vergunst, A.C., van Lier, M.C., den Dulk-Ras, A., Stuve, T.A., Ouwehand, A., and**
1118 **Hooykaas, P.J.** (2005). Positive charge is an important feature of the C-terminal
1119 transport signal of the VirB/D4-translocated proteins of Agrobacterium. Proc Natl Acad
1120 Sci U S A **102,** 832-837.
1121 **Wang, H., Han, S., Siao, W., Song, C., Xiang, Y., Wu, X., Cheng, P., Li, H., Jasik, J.,**
1122 **Micieta, K., Turna, J., Voigt, B., Baluska, F., Liu, J., Wang, Y., and Zhao, H.** (2015).
1123 Arabidopsis Synaptotagmin 2 Participates in Pollen Germination and Tube Growth and Is
1124 Delivered to Plasma Membrane via Conventional Secretion. Mol Plant **8,** 1737-1750.
1125 **Wang, P., Hawkins, T.J., Richardson, C., Cummins, I., Deeks, M.J., Sparkes, I., Hawes, C.,**
1126 **and Hussey, P.J.** (2014). The plant cytoskeleton, NET3C, and VAP27 mediate the link
1127 between the plasma membrane and endoplasmic reticulum. Curr Biol **24,** 1397-1405.
1128 **Wojtaszek, P., Anielska-Mazur, A., Gabrys, H., Baluska, F., and Volkmann, D.** (2005).
1129 Recruitment of myosin VIII towards plastid surfaces is root-cap specific and provides the
1130 evidence for actomyosin involvement in root osmosensing. Funct Plant Biol **32,** 721-736.

1131 **Wu, S.Z., and Bezanilla, M.** (2014). Myosin VIII associates with microtubule ends and together
1132 with actin plays a role in guiding plant cell division. Elife **3**.
1133 **Yang, L., Qin, L., Liu, G., Peremyslov, V.V., Dolja, V.V., and Wei, Y.** (2014). Myosins XI
1134 modulate host cellular responses and penetration resistance to fungal pathogens. Proc
1135 Natl Acad Sci U S A **111,** 13996-14001.
1136 **Yang, Q., Li, X., Tu, H., and Pan, S.Q.** (2017). Agrobacterium-delivered virulence protein
1137 VirE2 is trafficked inside host cells via a myosin XI-K-powered ER/actin network. Proc
1138 Natl Acad Sci U S A **114,** 2982-2987.
1139 **Yusibov, V.M., Steck, T.R., Gupta, V., and Gelvin, S.B.** (1994). Association of single-
1140 stranded transferred DNA from Agrobacterium tumefaciens with tobacco cells. Proc Natl
1141 Acad Sci U S A **91,** 2994-2998.
1142 **Zupan, J.R., Citovsky, V., and Zambryski, P.** (1996). Agrobacterium VirE2 protein mediates
1143 nuclear uptake of single-stranded DNA in plant cells. Proc Natl Acad Sci U S A **93,**
1144 2392-2397.
1145

1146

1147 **FIGURE LEGENDS**
1148
1149 **Figure 1. Some *Arabidopsis* actin and myosin genes are important for *Agrobacterium*-**
1150 **mediated transformation. (A)** Root segments from *Arabidopsis* wild-type and *act2-1*, *act7-1*,
1151 *act7-4*, *act12*, *act7*-4 comp (complemented), or *bot1* mutants were infected with *A. tumefaciens*
1152 A208 (tumorigenic strain for stable transformation; left panel) or *A. tumefaciens* At849 (T-DNA
1153 contains a plant-active *gusA*-intron gene for transient transformation; right panel). After two
1154 days, the root segments were moved to medium (MS lacking phytohormones for stable
1155 transformation, CIM for transient transformation) containing timentin to kill the bacteria. For
1156 stable transformation, the presence of tumors was scored one month after infection. For transient
1157 transformation, root segments were stained with X-gluc after an additional four days, and the
1158 percentage of roots showing GUS activity was calculated. *Act7-4* comp, *act7-4* mutant
1159 complemented with an *ACT7* cDNA. **(B and C)** Root segments from *Arabidopsis* wild-type and
1160 single or higher order *myosin VIII* or *XI* mutants were infected with *A. tumefaciens* At849
1161 transiently or *A. tumefaciens* A208 stably. A total of 10-15 plants and >100 segments per plant
1162 were tested for stable transformation. Values given are means ± SE. Asterisks indicate
1163 significant differences compared to wild-type plants. [*t-test*, $*P < 0.05$; $**P < 0.01$].
1164
1165 **Figure 2**. **All Myosin VIII family members can contribute to *Agrobacterium*-mediated**
1166 **transformation.** Root segments from transgenic *Arabidopsis* individually expressing either an
1167 empty vector or *myosin VIII* cDNAs in *myosin VIII-1/2/a/b* mutant plants **(A)**, or in wild-type
1168 plants **(B)**, were infected with *A. tumefaciens* At849. Transgenic *Arabidopsis* expressing cDNAs
1169 encoding *myosins VIII-2, VIII-A, VIII-B, VIII-2+VIII-B* or *VIII-A+VIII-B* in the *myosin VIII-*
1170 *1/2/a/b* mutant background **(C)** or in wild-type Col0 plants **(D)** were similarly infected with *A.*
1171 *tumefaciens* At849. Transient transformation efficiencies are indicated as the percentage of roots
1172 showing GUS activity six days after infection. A total of 10-15 plants and >100 segments per
1173 plant, from five independent transgenic lines, were tested for transient transformation. Values
1174 given are means ± SE Asterisks indicate significant differences compared to control plants that
1175 contain an empty vector (**A** and **B**), the *myosin VIII-1/2/a/b* quadruple mutant (**C**), or wild-type
1176 Col-0 plants (**D**). [*t-test*, $*P < 0.05$; $**P < 0.01$; $***P < 0.001$; $****P < 0.0001$].
1177
1178

1179 **Figure 3**. **Inducible expression of myosin VIII, but not the myosin XI-K, cargo binding**
1180 **domains (CBD) inhibits transient transformation.** Root segments from transgenic
1181 *Arabidopsis* expressing the cargo binding domain (CBD) of the indicated myosin protein, under
1182 the control of a β-estradiol inducible promoter, were treated with β-estradiol or control solutions
1183 for 24 hr before infection with *A. tumefaciens* At849. The percentage of roots showing GUS
1184 activity six days after infection indicates the transient transformation efficiency. A total of 10-15
1185 plants and >100 segments per plant, from five independent transgenic lines, were tested for
1186 transient transformation. Values given are means ± SE. Asterisks indicate significant
1187 differences compared to uninduced plants. [*t-test*, $^{**}P < 0.01$; $^{***}P < 0.001$].
1188

1189 **Figure 4**. **Expression of VirE2-Venus in the *myosin VIII-1/2/a/b* mutant cannot**
1190 **complement a *virE2* mutant *Agrobacterium* strain for transient transformation. (A)**
1191 *Agrobacterium*-mediated transient transformation assays were conducted on roots of four
1192 independent transgenic lines of wild-type (Lines 2, 4, 5 and 8) or **(B)** the *myosin VIII-1/2/a/b*
1193 mutant (Lines 2, 3, 12, and 13). Root segments were inoculated with 10^6, 10^7, or 10^8 cfu/ml of
1194 the *virE2* mutant strain *A. tumefaciens* At1879 containing the T-DNA binary vector pBISN2.
1195 Plants were treated with β-estradiol (gray bars) or control solution (black bars) for VirE2-Venus
1196 expression 24 hr before infection. The percentage of roots showing GUS activity was calculated
1197 as in Figure 1. A total of 10-15 plants from each line and >100 segments per plant were tested
1198 for transient transformation. Values given are means ± SE. Asterisks indicate significant
1199 differences compared to uninduced plants. [*t-test*, $^{*}P < 0.05$; $^{**}P < 0.01$]. **(C)** Confocal images
1200 showing aggregation of VirE2-Venus proteins in transgenic roots of either wild-type (top panel)
1201 or *myosin VIII 1/2/a/b* mutant backgrounds (bottom panel). **(D)** Quantitative analysis of the size
1202 of VirE2-Venus aggregates and the percentage of the cellular area occupied by the aggregates.
1203 Image J was used for analysis. The average VirE2-Venus aggregate size was 2.0±0.3 μm^2 in
1204 wild-type roots, and 6.2±0.6 μm^2 in *myosin VIII-1/2/a/b* quadruple mutant roots. **(E)** Western
1205 blot detection of VirE2-Venus proteins expressed in transgenic plants of either the Col-0 or the
1206 *myosin VIII-1/2/a/b* quadruple myosin mutant background. Mouse anti-GFP antibody was used
1207 to detect VirE2-Venus protein expressed after induction of individual transgenic lines. The

1208 house-keeping protein phosphoenolpyruvate carboxylase (PEPC) was detected using a rabbit
1209 anti-PEPC antibody and served as an internal control.

1210 **Figure 5**. **Analysis of VirE2-Venus aggregates in roots of transgenic *Arabidopsis* expressing**
1211 **the CBDs of various Myosin VIII proteins.** Roots were treated with β-estradiol for eight hr.
1212 Random areas of confocal images from roots expressing **(A)** Myosin VIII-1 or VIII-2 CBDs, or
1213 **(B)** Myosin VIII-A or VIII-B CBDs were analyzed using Image J. Both the sizes and the
1214 percentage of the cellular area occupied by the VirE2-Venus aggregates are shown.

1215 **Figure 6**. **VirE2-Venus interacts with some myosin cargo binding domains (CBDs) *in vitro*.**
1216 VirE2-Venus or Venus proteins were incubated with the indicated myc-tagged myosin CBD,
1217 VIP1, or Lamin C. Following binding to anti-GFP beads, proteins were eluted and subjected to
1218 Western blot analysis using anti-myc antibodies. Coomassie stained gels are shown in panels **A**,
1219 **C**, and **E**, and immunoblots in panels **B**, **D**, and **F**. VirE2-Venus interacts with the CBDs of
1220 myosins VIII-2, VIII-A, VIII-B, and XI-K, and with VIP1 (panels **B**, **D**, and **F**), but not with the
1221 CBD of myosin VIII-1 or with Lamin C (panels **D** and **F**). Venus, as a negative control, does not
1222 interact with any myc-tagged protein.

1223 **Figure 7**. **The cargo binding domains (CBD) of some myosins interact with VirE2 in yeast.**
1224 Yeast two-hybrid analysis was conducted with VirE2 as the bait and individual myosin CBDs as
1225 the prey. Following co-transformation of the bait and prey plasmids, single colonies were picked
1226 and serial dilutions of yeast were grown on **(A)** SD-Trp-Leu (-TL) medium, or **(B)** SD-Trp-Leu-
1227 His medium supplemented with 3 mM 3-amino-1,2,4-triazole (-TLH+3AT). Colony growth on
1228 SD-TLH+3AT indicates interaction between VirE2 and the myosin CBD. VIP1 was used as a
1229 positive control for interaction with VirE2. Lamin C and the empty vector were used as negative
1230 controls. SD, synthetic dropout medium.

1231 **Figure 8**. **Myosin cargo binding domains can form complexes with VirE2 when expressed**
1232 **in *Arabidopsis*.** **(A)** Protein extracts from roots of transgenic *Arabidopsis* plants expressing
1233 VirE2-Venus, or Venus, and the indicated myc-tagged myosin CBD transgenes were incubated
1234 with anti-GFP beads, the bound proteins eluted, and subjected to Western blot analysis using
1235 anti-myc antibodies. Myc-tagged VIP1 was used as a positive control. **(B)** Root extracts

1236 expressing VirE2-Venus or Venus and myc-tagged myosin VIII-2 CBD were incubated with
1237 anti-GFP beads, the bound proteins eluted, and subjected to Western blot analysis using anti-myc
1238 antibodies.

1239 **Figure 9**. **Co-localization of VirE2-Venus and mCherry-Myosins in *Arabidopsis* roots.**
1240 Roots of transgenic *Arabidopsis* plants containing VirE2-Venus and mCherry-myosin genes,
1241 each under the control of a β-estradiol-inducible promoter, were treated with β-estradiol for 8 hr
1242 and examined by confocal microscopy. Bars indicate 50 μm.

1243 **Figure 10**. **Bimolecular fluorescence complementation (BiFC) of VirE2 with various**
1244 **myosin full-length proteins in *Arabidopsis* roots.** Transgenic *Arabidopsis* plants containing
1245 VirE2-cEYFP and the indicated myosin-nVenus constructs, each under the control of a β-
1246 estradiol-inducible promoter, as well as mCherry-ABD2 were treated with β-estradiol for 48 hr
1247 and the fluorescence signal detected by confocal microscopy. VirE2 interacts with the CBDs of
1248 myosins VIII-2, VIII-A, and VIII-B. VirE2 does not interact with the myosin VIII-1. Yellow
1249 fluorescence indicates interaction of VirE2-Venus with the myosin CBD. Actin filaments are
1250 labeled by mCherry-ABD2. Bars indicate 50 μm.
1251

1252 **Figure 11**. **Incubation of *Arabidopsis* roots with *Agrobacterium* that can transfer T-DNA**
1253 **results in increased VirE2-Venus in the perinuclear region. (A)** Transgenic *Arabidopsis*
1254 plants containing an inducible *VirE2-Venus* transgene were treated with 5 μm β-estradiol for 24
1255 hr, followed by inoculation with 10^8 cfu/ml of the *virE2* mutant *A. tumefaciens* At1872 without a
1256 binary vector (At2403, left panel) or with T-DNA on a binary vector (At2404, right panel). The
1257 percentage of total VirE2-Venus fluorescence in the perinuclear area was calculated. Images of
1258 10-15 transgenic lines and >50 cells were analyzed. The data indicate means ± SE. Asterisks
1259 indicate significant differences between roots inoculated with the two *Agrobacterium* strains.
1260 **(B-F)** the relative distribution of VirE2-Venus at the cell poles or in the cytoplasm following
1261 infection with *A. tumefaciens* At2403 or At2404 of roots co-expressing CBDs of myosin VIiI-1.
1262 myosin VIII-2, myosin VIII-A, myosin VIII-B, or myosin XI-K (B, C, D, E, F, respectively).
1263 Images of 10-15 transgenic lines and >50 cells were analyzed. The data indicate means ± SE.

1264 Asterisks indicate significant differences between roots inoculated with the two *Agrobacterium*
1265 strains. [*t-test*, $*P < 0.05$; $**P < 0.01$; $***P < 0.001$].
1266
1267 **Figure 12**. **Loss of function of myosin XI-K, but not myosin VIII, disrupts movement of**
1268 **VirE2-Venus along actin filaments.** Transgenic plants expressing mCherry-ABD2
1269 constitutively and VirE2-Venus inducibly in Col-0, *myosin VIII-1/2/a/b*, and myosin XI-K CBD
1270 plants were used in this experiment. Roots of these plants were treated with 10 μm β-estradiol
1271 for 8 hr. Time lapse images were taken by confocal microscopy. Four images of each field are
1272 shown at the indicated times (0, 60, 90, and 120 seconds). Blue arrows indicate the initial
1273 position of a particular VirE2-Venus aggregate; white arrows indicate the position of the same
1274 aggregate at various times thereafter. Bars indicate 5 μm.
1275
1276 **Figure 13. VirE2-iGFP11 delivered from *Agrobacterium* localizes to the periphery of**
1277 ***Arabidopsis* cells and along filaments. (A)** *Arabidopsis* leaves expressing GFP1-10 were
1278 infiltrated with an *Agrobacterium* strain expressing VirE2-iGFP11. The leaves were imaged one
1279 day later by confocal microscopy. **(B)** Non-infiltrated leaves of *Arabidopsis* expressing GFP1-
1280 10. Red arrows indicate VirE2 along cytoplasmic filaments. Bars indicate 50 μm.
1281
1282 **Figure 14**. **Model of myosin VIII and myosin XI-K involvement in VirE2 trafficking to the**
1283 **perinuclear region. (A)** *Agrobacterium* virulence effector proteins, including VirE2 and VirE3,
1284 are secreted into host cells through a Type IV secretion system. VirE2 and VirE3 interact at the
1285 plant plasma membrane. Myosin VIII proteins localize at the plasma membrane and help tether
1286 VirE2 to the plasma membrane when no T-DNA is present. **(B)** When T-strands (as a VirD2/T-
1287 strand complex) enter the host cell, VirE2 molecules are released and some may bind T-DNA,
1288 following which VirE2 interacts with myosin XI-K and moves along actin filaments to the
1289 perinuclear region. Not shown are the *Agrobacterium* virulence effector proteins VirD5 and
1290 VirF which also are transferred to the plant.
1291
1292

1293 **Table 1.** Velocity of VirE2-Venus movement in leaf and root cells of various *Arabidopsis*
1294 transgenic lines

Transgene(s) in plant/ *Agrobacterium* infection[a]	***Arabidopsis* background**	**Velocity in leaves (µm/sec)**	**Velocity in roots (µm/sec)**
VirE2-Venus	Col-0	0.353± 0.06	0.312± 0.07
VirE2-Venus	myosin *VIII-1/2/a/b*	0.378± 0.02	0.318± 0.02
VirE2-Venus + Myosin VIII-1 CBD	Col-0	0.407 ± 0.06	0.341 ± 0.04
VirE2-Venus + Myosin VIII-2 CBD	Col-0	0.398 ± 0.07	0.321 ± 0.02
VirE2-Venus + Myosin VIII-A CBD	Col-0	0.387 ± 0.07	0.304 ± 0.01
VirE2-Venus + Myosin VIII-B CBD	Col-0	0.401 ± 0.05	0.328 ± 0.04
VirE2-Venus + Myosin XI-K CBD	Col-0	Not detectable	Not detectable
VirE2-Venus + Myosin XI-K CBD + *Agrobacterium* (- T-DNA)	Col-0	Not detectable	Not detectable
VirE2-Venus + Myosin XI-K CBD + *Agrobacterium* (+ T-DNA)	Col-0	Not detectable	Not detectable
Agrobacterium VirE2-iGFP11[b]	Col-0 GFP1-10	0.323 ± 0.08	-----

1295 [a]All transgenes are under the control of a β-estradiol-inducible promoter; CBD, cargo binding
1296 domain. >50 cells of 10 independent transgenic lines were examined for each genotype of
1297 transgenic plant.
1298 [b]Measurements were conducted on 19 VirE2 aggregates within 10 cells.

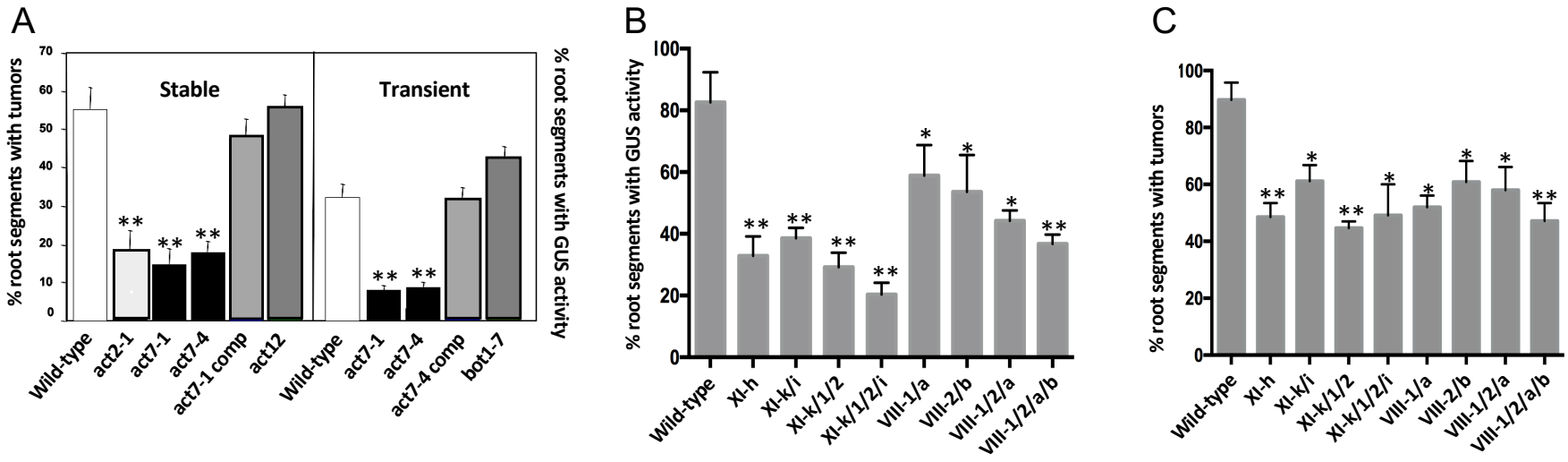

Figure 1. Some *Arabidopsis* actin and myosin genes are important for *Agrobacterium*-mediated root transformation. **(A)** Root segments from *Arabidopsis* wild-type and *act2-1*, *act7-1*, act7-4, *act12*, *act7*-4 comp, or *bot1* mutants were infected with *A. tumefaciens* A208 (tumorigenic strain for stable transformation; left panel) or *A. tumefaciens* At849 (T-DNA contains a plant-active *gusA*-intron gene for transient transformation; right panel). After two days, the root segments were moved to medium (MS lacking phytohormones for stable transformation, CIM for transient transformation) containing timentin to kill the bacteria. For stable transformation, the presence of tumors was scored one month after infection. For transient transformation, root segments were stained with X-gluc after an additional four days, and the percentage of roots showing GUS activity was calculated. *act7-4* comp, *act7-4* mutant complemented with an *ACT7* cDNA. **(B and C)** Root segments from *Arabidopsis* wild-type and single or higher order *myosin VIII* or *XI* mutants were infected with *A. tumefaciens* At849 transiently or *A. tumefaciens* A208 stably. A total of 10-15 plants and >100 segments per plant were tested for stable transformation. Values given are means ± SE. Asterisks indicate significant differences compared to wild-type plants. [*t-test*, $*P < 0.05$; $**P < 0.01$].

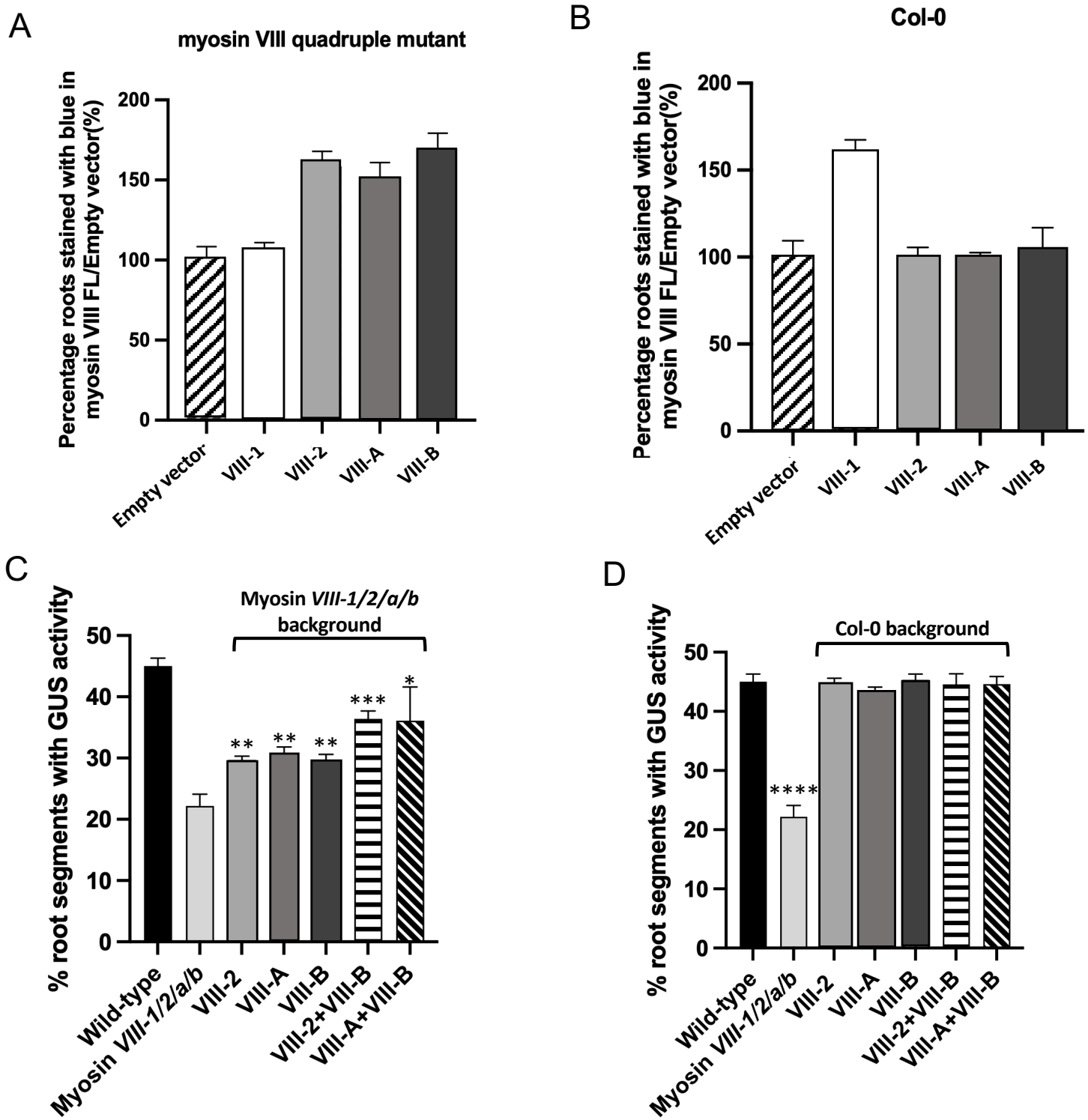
A
myosin VIII quadruple mutant
Percentage roots stained with blue in myosin VIII FL/Empty vector(%)
200
150
100
50
0
Empty vector
VIII-1
VIII-2
VIII-A
VIII-B
B
Col-0
Percentage roots stained with blue in myosin VIII FL/Empty vector(%)
200
150
100
50
0
Empty vector
VIII-1
VIII-2
VIII-A
VIII-B
C
Myosin VIII-1/2/a/b background
% root segments with GUS activity
50
40
30
20
10
0
**
**
**
***
*
Wild-type
Myosin VIII-1/2/a/b
VIII-2
VIII-A
VIII-B
VIII-2+VIII-B
VIII-A+VIII-B
D
Col-0 background
% root segments with GUS activity
50
40
30
20
10
0
****
Wild-type
Myosin VIII-1/2/a/b
VIII-2
VIII-A
VIII-B
VIII-2+VIII-B
VIII-A+VIII-B

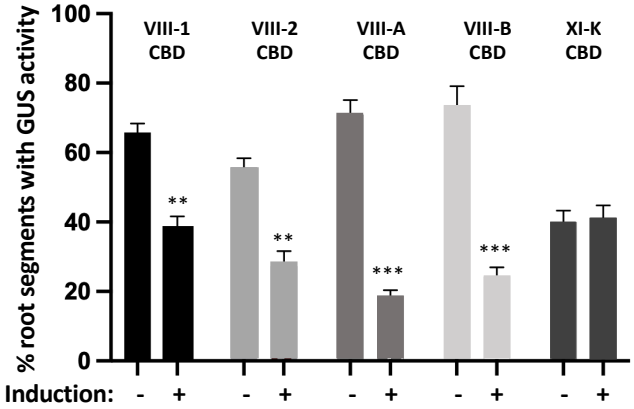

Figure 3. **Inducible expression of myosin VIII, but not the myosin XI-K, cargo binding domains (CBD) inhibits transient transformation.** Root segments from transgenic *Arabidopsis* expressing the cargo binding domain (CBD) of the indicated myosin protein, under the control of a β-estradiol inducible promoter, were treated with β-estradiol or control solutions for 24 hr before infection with *A. tumefaciens* At849. The percentage of roots showing GUS activity six days after infection indicates the transient transformation efficiency. A total of 10-15 plants and >100 segments per plant, from five independent transgenic lines, were tested for transient transformation. Values given are means ± SE. Asterisks indicate significant differences compared to uninduced plants. [*t-test*, $^{**}P < 0.01$; $^{***}P < 0.001$].

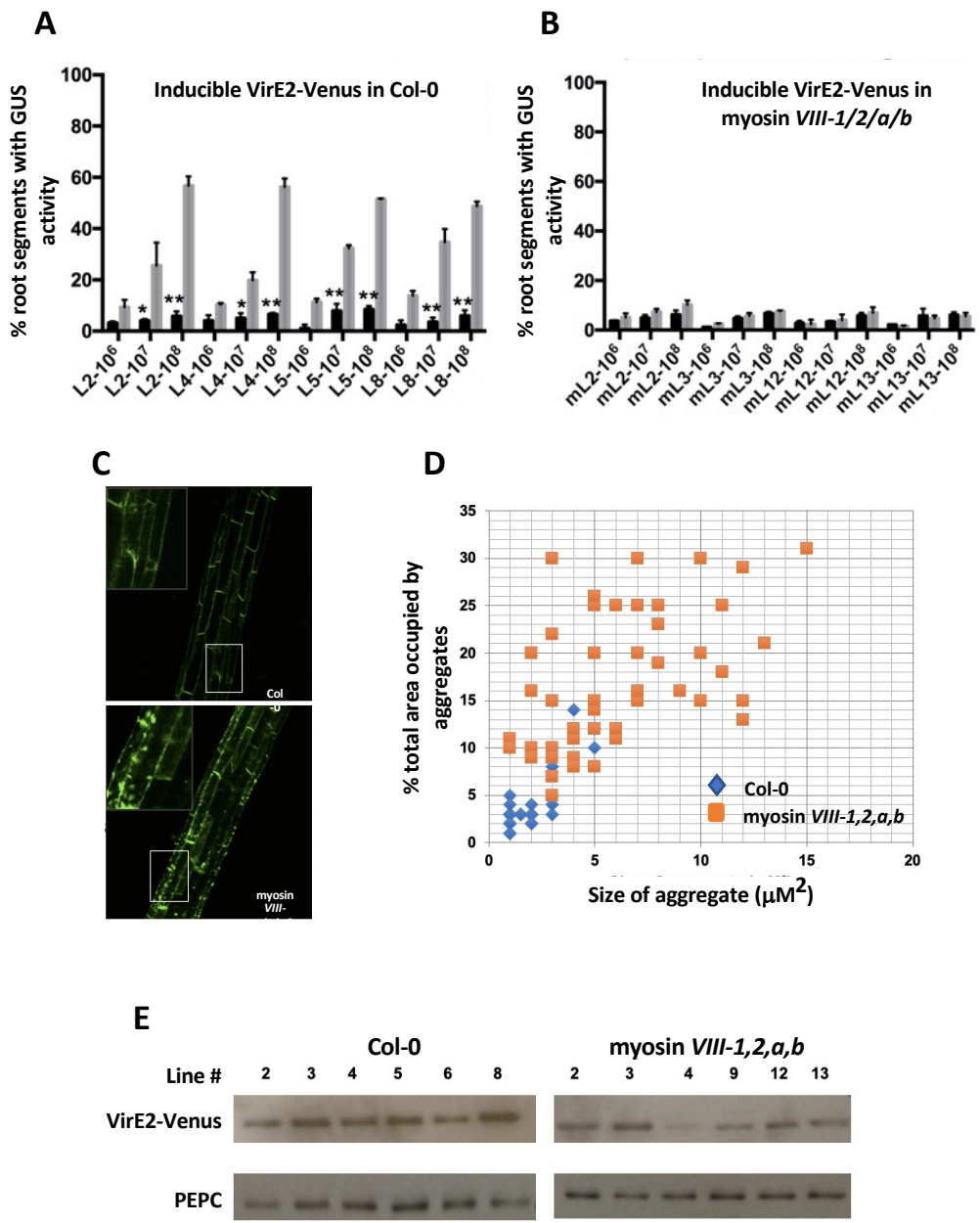
A
Inducible VirE2-Venus in Col-0
% root segments with GUS activity
100
80
60
40
20
0
L2-10^6
L2-10^7
L2-10^8
L4-10^6
L4-10^7
L4-10^8
L5-10^6
L5-10^7
L5-10^8
L8-10^6
L8-10^7
L8-10^8
B
Inducible VirE2-Venus in myosin VIII-1/2/a/b
% root segments with GUS activity
mL2-10^6
mL2-10^7
mL2-10^8
mL3-10^6
mL3-10^7
mL3-10^8
mL12-10^6
mL12-10^7
mL12-10^8
mL13-10^6
mL13-10^7
mL13-10^8
C
Col -0
myosin VIII-
D
% total area occupied by aggregates
Size of aggregate (μM^2)
Col-0
myosin VIII-1,2,a,b
E
Col-0
myosin VIII-1,2,a,b
Line #
2 3 4 5 6 8
2 3 4 9 12 13
VirE2-Venus
PEPC

- **Figure 4**. **Expression of VirE2-Venus in the *myosin VIII-1/2/a/b* mutant cannot complement a *virE2* mutant *Agrobacterium* strain for transient transformation.** **(A)** *Agrobacterium*-mediated transient transformation assays were conducted on roots of four independent transgenic lines of wild-type (Lines 2, 4, 5 and 8) or **(B)** the *myosin VIII-1/2/a/b* mutant (Lines 2, 3, 12, and 13). Root segments were inoculated with 10^6, 10^7, or 10^8 cfu/ml of the *virE2* mutant strain *A. tumefaciens* At1879 containing the T-DNA binary vector pBISN2. Plants were treated with β-estradiol (gray bars) or control solution (black bars) for VirE2-Venus expression 24 hr before infection. The percentage of roots showing GUS activity was calculated as in Figure 1. A total of 10-15 plants from each line and >100 segments per plant were tested for transient transformation. Values given are means ± SE. Asterisks indicate significant differences compared to uninduced plants. [*t-test*, $*P < 0.05$; $**P < 0.01$]. **(C)** Confocal images showing aggregation of VirE2-Venus proteins in transgenic roots of either wild-type (top panel) or *myosin VIII 1/2/a/b* mutant backgrounds (bottom panel). **(D)** Quantitative analysis of the size of VirE2-Venus aggregates and the percentage of the cellular area occupied by the aggregates. Image J was used for analysis. The average VirE2-Venus aggregate size was 2.0±0.3 μm^2 in wild-type roots, and 6.2±0.6 μm^2 in *myosin VIII-1/2/a/b* quadruple mutant roots. **(E)** Western blot detection of VirE2-Venus proteins expressed in transgenic plants of either the Col-0 or the *myosin VIII-1/2/a/b* quadruple myosin mutant background. Mouse anti-GFP antibody was used to detect VirE2-Venus protein expressed after induction of individual transgenic lines. The house-keeping protein phosphoenolpyruvate carboxylase (PEPC) was detected using a rabbit anti-PEPC antibody and served as an internal control.

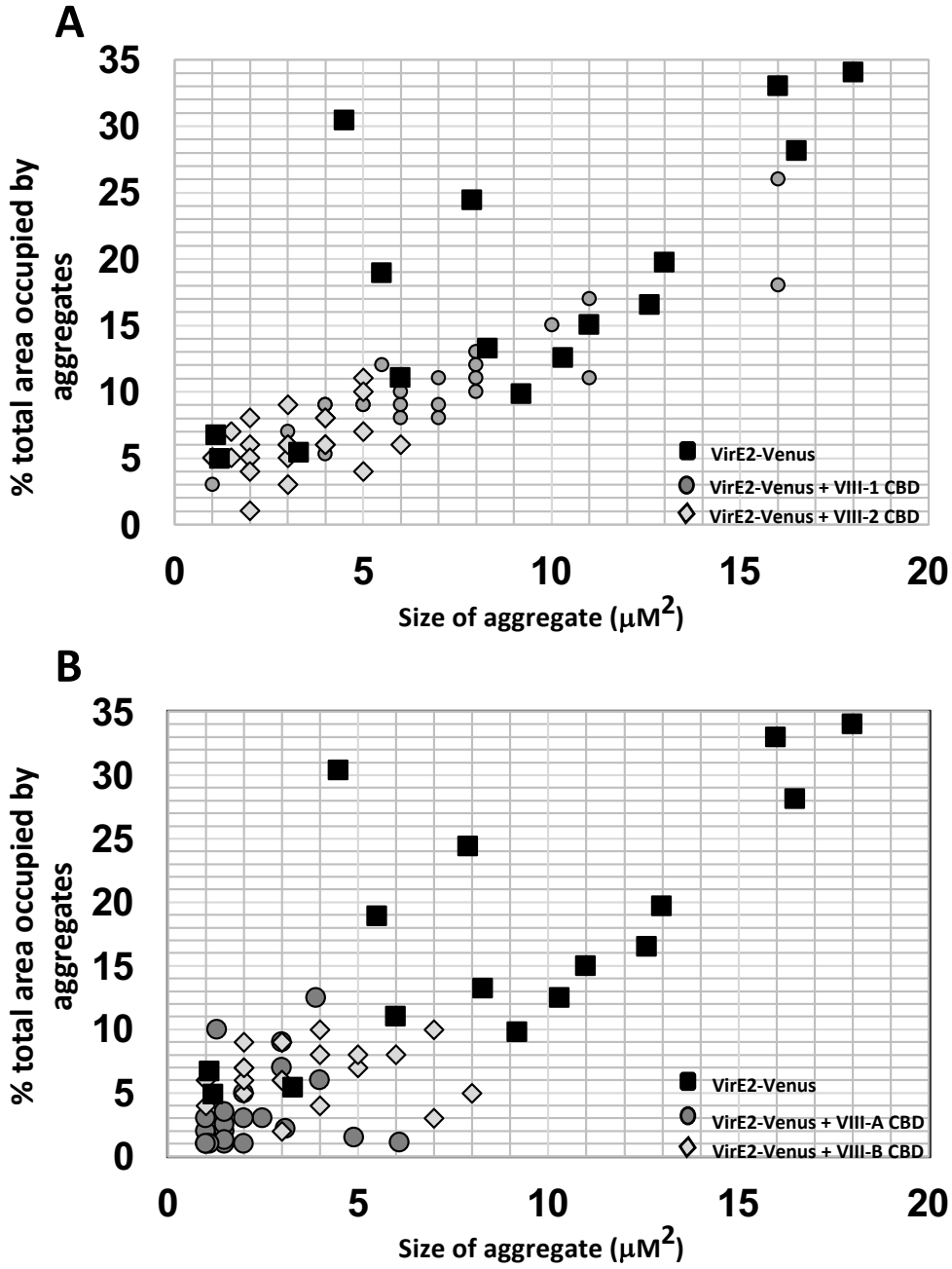

Figure 5. **Analysis of VirE2-Venus aggregates in roots of transgenic *Arabidopsis* expressing the CBDs of various Myosin VIII proteins.** Roots were treated with β-estradiol for eight hr. Random areas of confocal images from roots expressing **(A)** Myosin VIII-1 or VIII-2 CBDs, or **(B)** Myosin VIII-A or VIII-B CBDs were analyzed using Image J. Both the sizes and the percentage of the cellular area occupied by the VirE2-Venus aggregates are shown.

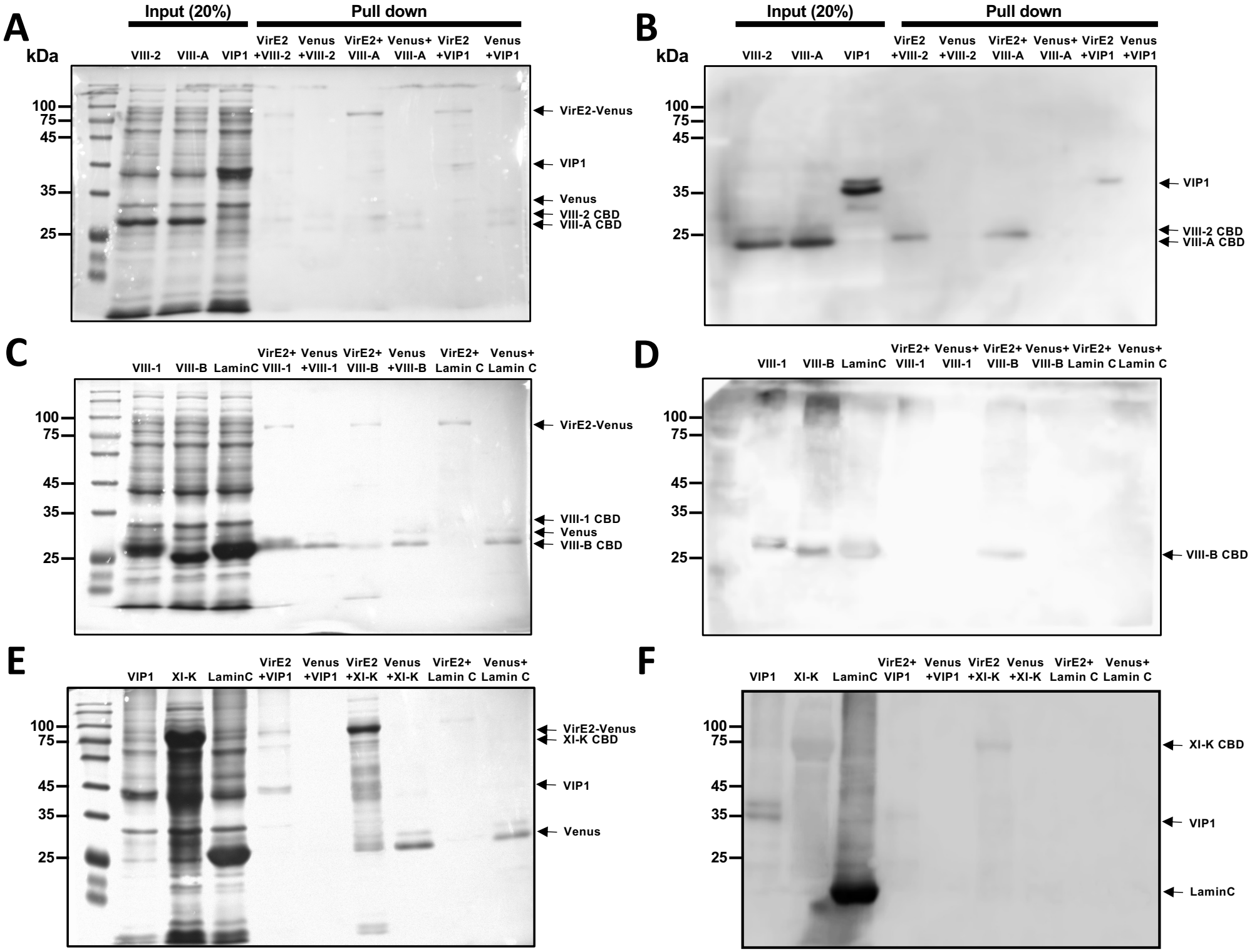
A
Input (20%)
Pull down
kDa
VIII-2
VIII-A
VIP1
VirE2 +VIII-2
Venus +VIII-2
VirE2+ VIII-A
Venus+ VIII-A
VirE2 +VIP1
Venus +VIP1
100
75
45
35
25
VirE2-Venus
VIP1
Venus
VIII-2 CBD
VIII-A CBD
B
Input (20%)
Pull down
kDa
VIII-2
VIII-A
VIP1
VirE2 +VIII-2
Venus +VIII-2
VirE2+ VIII-A
Venus+ VIII-A
VirE2 +VIP1
Venus +VIP1
100
75
45
35
25
VIP1
VIII-2 CBD
VIII-A CBD
C
VIII-1
VIII-B
LaminC
VirE2+ VIII-1
Venus +VIII-1
VirE2+ VIII-B
Venus +VIII-B
VirE2+ Lamin C
Venus+ Lamin C
100
75
45
35
25
VirE2-Venus
VIII-1 CBD
Venus
VIII-B CBD
D
VIII-1
VIII-B
LaminC
VirE2+ VIII-1
Venus+ VIII-1
VirE2+ VIII-B
Venus+ VIII-B
VirE2+ Lamin C
Venus+ Lamin C
100
75
45
35
25
VIII-B CBD
E
VIP1
XI-K
LaminC
VirE2 +VIP1
Venus +VIP1
VirE2 +XI-K
Venus +XI-K
VirE2+ Lamin C
Venus+ Lamin C
100
75
45
35
25
VirE2-Venus
XI-K CBD
VIP1
Venus
F
VIP1
XI-K
LaminC
VirE2+ VIP1
Venus +VIP1
VirE2 +XI-K
Venus +XI-K
VirE2+ Lamin C
Venus+ Lamin C
100
75
45
35
25
XI-K CBD
VIP1
LaminC

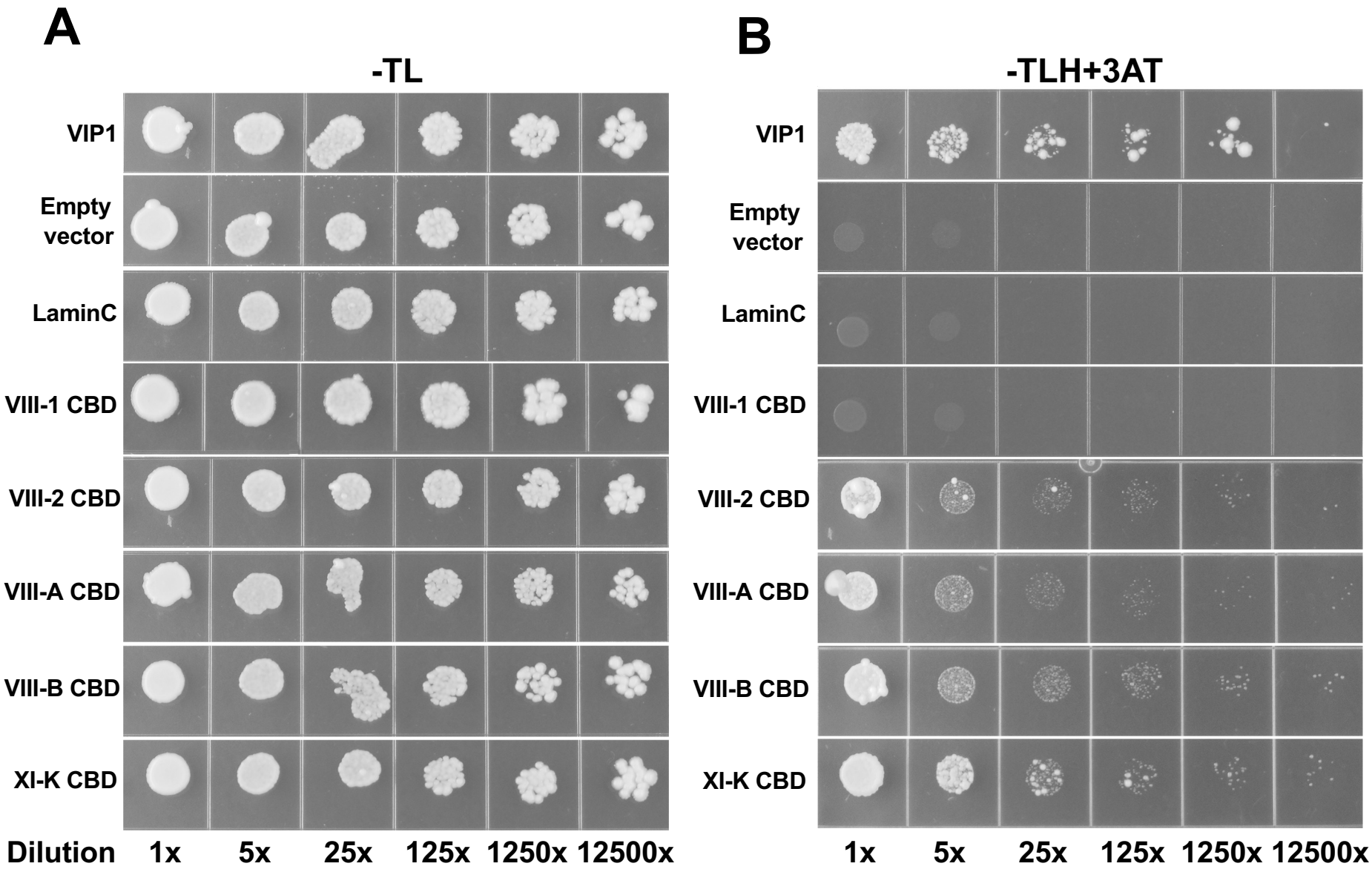

Figure 7. The cargo binding domains (CBD) of some myosins interact with VirE2 in yeast. Yeast two-hybrid analysis was conducted with VirE2 as the bait and individual myosin CBDs as the prey. Following co-transformation of the bait and prey plasmids, single colonies were picked and serial dilutions of yeast were grown on **(A)** SD-Trp-Leu (-TL) medium, or **(B)** SD-Trp-Leu-His medium supplemented with 3 mM 3-amino-1,2,4-triazole (-TLH+3AT). Colony growth on SD-TLH+3AT indicates interaction between VirE2 and the myosin CBD. VIP1 was used as a positive control for interaction with VirE2. Lamin C and the empty vector were used as negative controls. SD, synthetic dropout medium.

Figure 6. **VirE2-Venus interacts with some myosin cargo binding domains (CBDs) *in vitro*.** VirE2-Venus or Venus proteins were incubated with the indicated myc-tagged myosin CBD, VIP1, or Lamin C. Following binding to anti-GFP beads, proteins were eluted and subjected to Western blot analysis using anti-myc antibodies. Coomassie stained gels are shown in panels **A**, **C**, and **E**, and immunoblots in panels **B**, **D**, and **F**. VirE2-Venus interacts with the CBDs of myosins VIII-2, VIII-A, VIII-B, and XI-K, and with VIP1 (panels **B**, **D**, and **F**), but not with the CBD of myosin VIII-1 or with Lamin C (panels **D** and **F**). Venus, as a negative control, does not interact with any myc-tagged protein.

Figure 2. **All Myosin VIII family members can contribute to *Agrobacterium*-mediated transformation.** Root segments from transgenic *Arabidopsis* individually expressing either an empty vector or *myosin VIII* cDNAs in *myosin VIII-1/2/a/b* mutant plants **(A)**, or in wild-type plants **(B)**, were infected with *A. tumefaciens* At849. Transgenic *Arabidopsis* expressing cDNAs encoding *myosins VIII-2, VIII-A, VIII-B, VIII-2+VIII-B* or *VIII-A+VIII-B* in the *myosin VIII-1/2/a/b* mutant background **(C)** or in wild-type Col-0 plants **(D)** were similarly infected with *A. tumefaciens* At849. Transient transformation efficiencies are indicated as the percentage of roots showing GUS activity six days after infection. A total of 10-15 plants and >100 segments per plant, from five independent transgenic lines, were tested for transient transformation. Values given are means ± SE. Asterisks indicate significant differences compared to control plants that contain an empty vector (**A** and **B**), the *myosin VIII-1/2/a/b* quadruple mutant (**C**), or wild-type Col-0 plants (**D**). [*t-test*, $*P < 0.05$; $**P < 0.01$; $***P < 0.001$; $****P < 0.0001$].

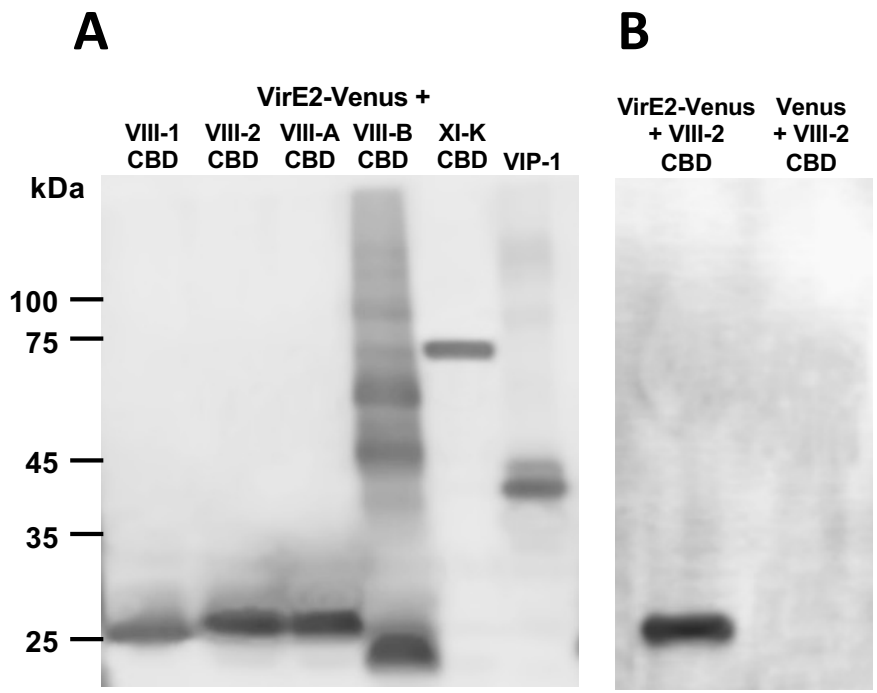

Figure 8. **Myosin cargo binding domains can form complexes with VirE2 when expressed in *Arabidopsis*. (A)** Protein extracts from roots of transgenic *Arabidopsis* plants expressing VirE2-Venus, or Venus, and the indicated myc-tagged myosin CBD transgenes were incubated with anti-GFP beads, the bound proteins eluted, and subjected to Western blot analysis using anti-myc antibodies. Myc-tagged VIP1 was used as a positive control. **(B)** Root extracts expressing VirE2-Venus or Venus and myc-tagged myosin VIII-2 CBD were incubated with anti-GFP beads, the bound proteins eluted, and subjected to Western blot analysis using anti-myc antibodies.

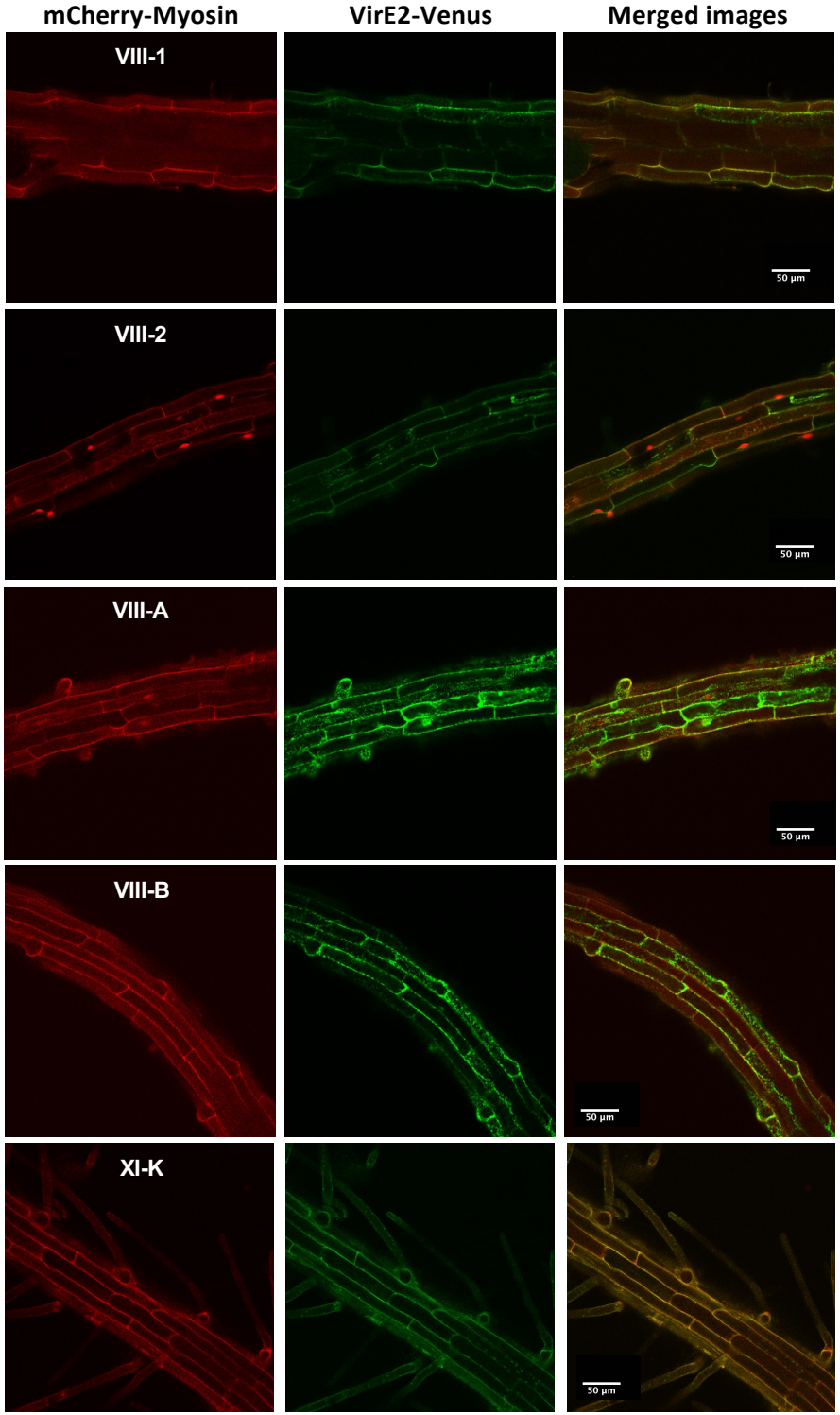
mCherry-Myosin
VirE2-Venus
Merged images
VIII-1
VIII-2
VIII-A
VIII-B
XI-K
50 µm

Figure 9. **Co-localization of VirE2-Venus and mCherry-Myosins in *Arabidopsis* roots.** Roots of transgenic *Arabidopsis* plants containing VirE2-Venus and mCherry-myosin genes, each under the control of a β-estradiol-inducible promoter, were treated with β-estradiol for 8 hr and examined by confocal microscopy. Bars indicate 50 μm.

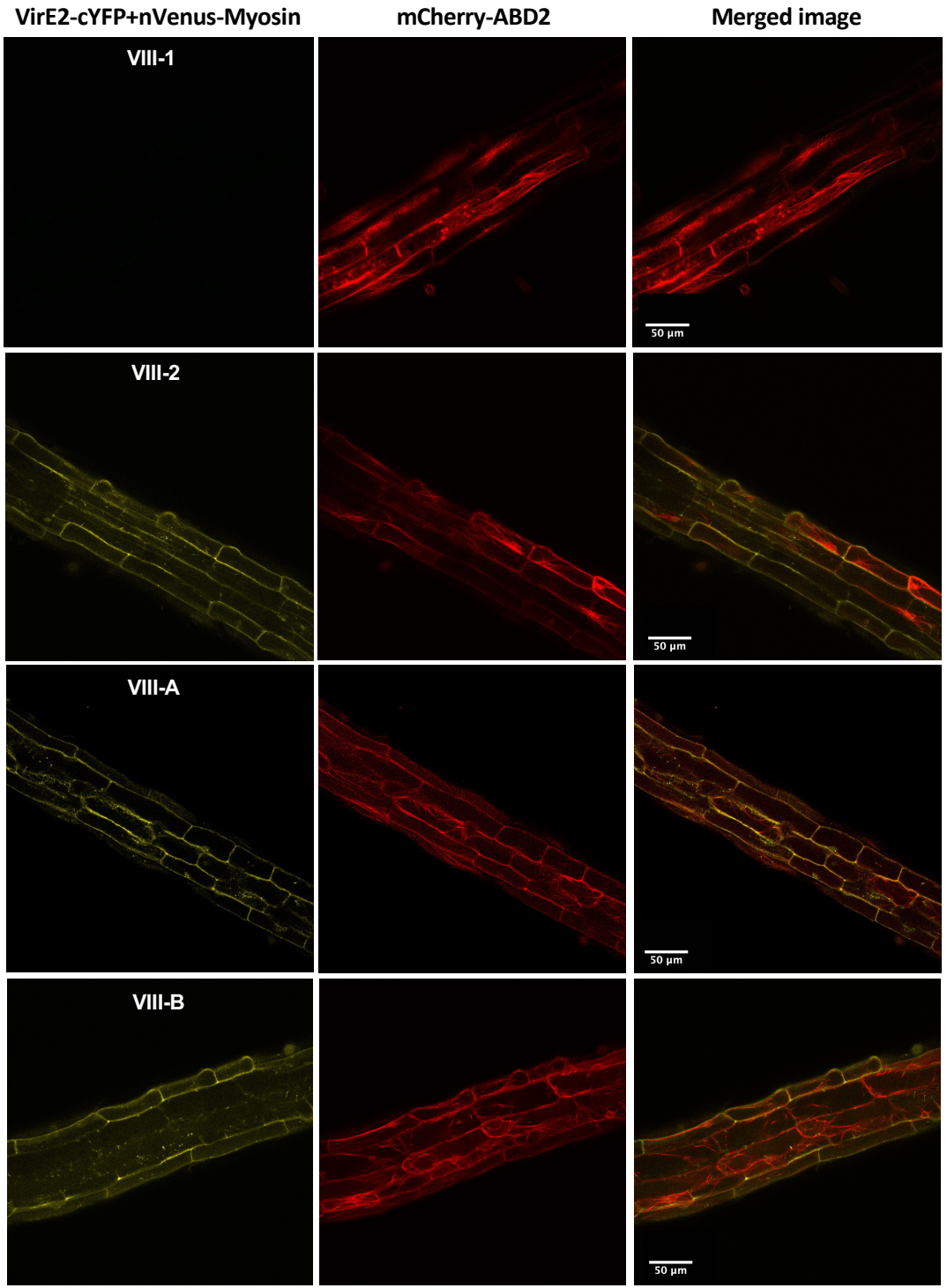
VirE2-cYFP+nVenus-Myosin
mCherry-ABD2
Merged image
VIII-1
VIII-2
VIII-A
VIII-B
50 µm
50 µm
50 µm
50 µm

Figure 10. **Bimolecular fluorescence complementation (BiFC) of VirE2 with various myosin full-length proteins in *Arabidopsis* roots.** Transgenic *Arabidopsis* plants containing VirE2-cEYFP and the indicated myosin-nVenus constructs, each under the control of a β-estradiol-inducible promoter, as well as mCherry-ABD2 were treated with β-estradiol for 48 hr and the fluorescence signal detected by confocal microscopy. VirE2 interacts with the CBDs of myosins VIII-2, VIII-A, and VIII-B. VirE2 does not interact with the myosin VIII-1. Yellow fluorescence indicates interaction of VirE2-Venus with the myosin CBD. Actin filaments are labeled by mCherry-ABD2. Bars indicate 50 μm.

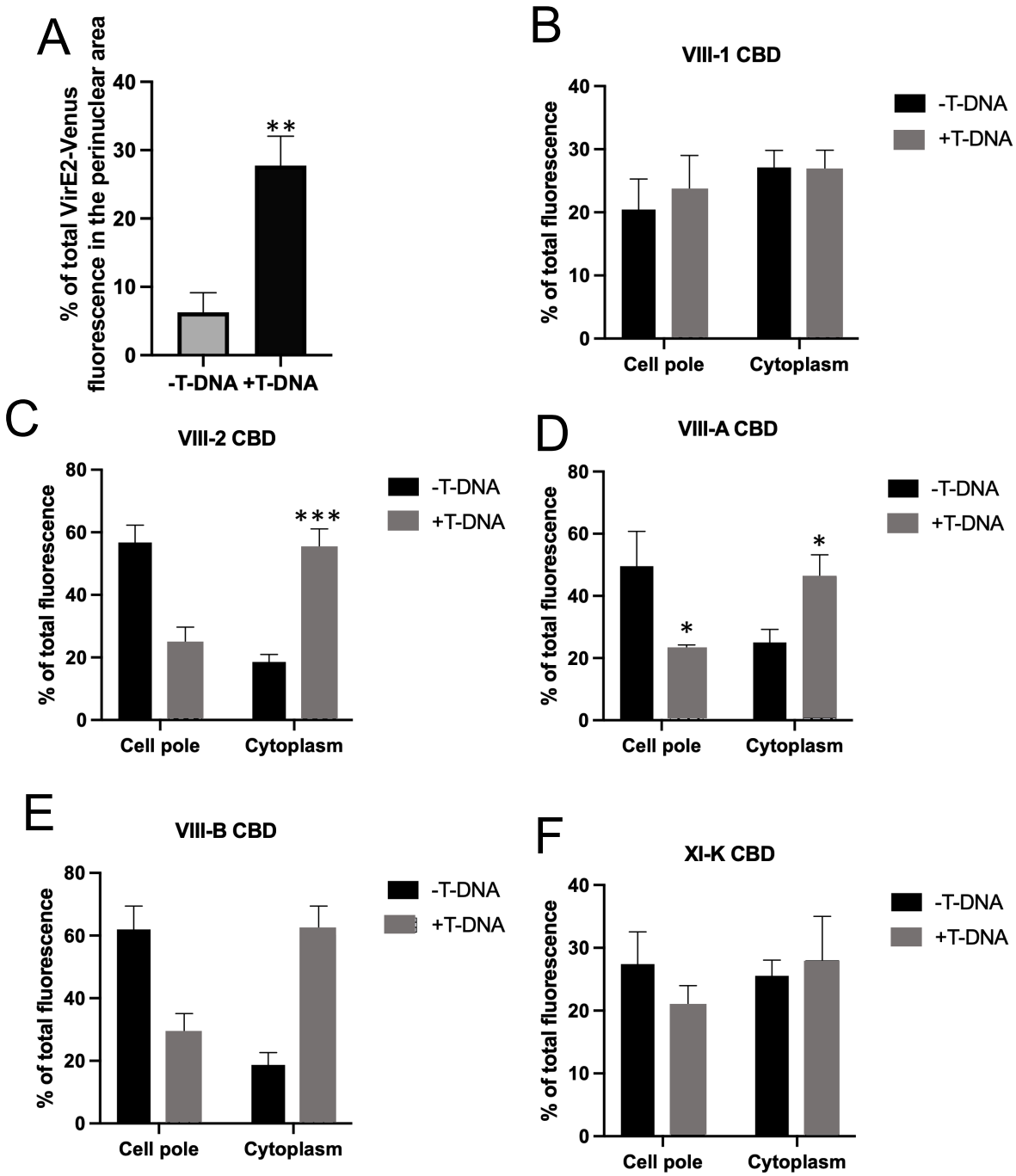
A
% of total VirE2-Venus fluorescence in the perinuclear area
40
30
20
10
0
**
-T-DNA +T-DNA
B
VIII-1 CBD
% of total fluorescence
-T-DNA
+T-DNA
Cell pole
Cytoplasm
C
VIII-2 CBD
80
60
40
20
0
***
D
VIII-A CBD
*
*
E
VIII-B CBD
F
XI-K CBD

Figure 11. **Incubation of *Arabidopsis* roots with *Agrobacterium* that can transfer T-DNA results in increased VirE2-Venus in the perinuclear region. (A)** Transgenic *Arabidopsis* plants containing an inducible *VirE2-Venus* transgene were treated with 5 μm β-estradiol for 24 hr, followed by inoculation with 10^8 cfu/ml of the *virE2* mutant *A. tumefaciens* At1872 without a binary vector (At2403, left panel) or with T-DNA on a binary vector (At2404, right panel). The percentage of total VirE2-Venus fluorescence in the perinuclear area was calculated. Images of 10-15 transgenic lines and >50 cells were analyzed. The data indicate means ± SE. Asterisks indicate significant differences between roots inoculated with the two *Agrobacterium* strains. **(B-F)** the relative distribution of VirE2-Venus at the cell poles or in the cytoplasm following infection with *A. tumefaciens* At2403 or At2404 of roots co-expressing CBDs of myosin VIII-1. myosin VIII-2, myosin VIII-A, myosin VIII-B, or myosin XI-K (B, C, D, E, F, respectively). Images of 10-15 transgenic lines and >50 cells were analyzed. The data indicate means ± SE. Asterisks indicate significant differences between roots inoculated with the two *Agrobacterium* strains. [*t-test*, $*P < 0.05$; $**P < 0.01$; $***P < 0.001$].

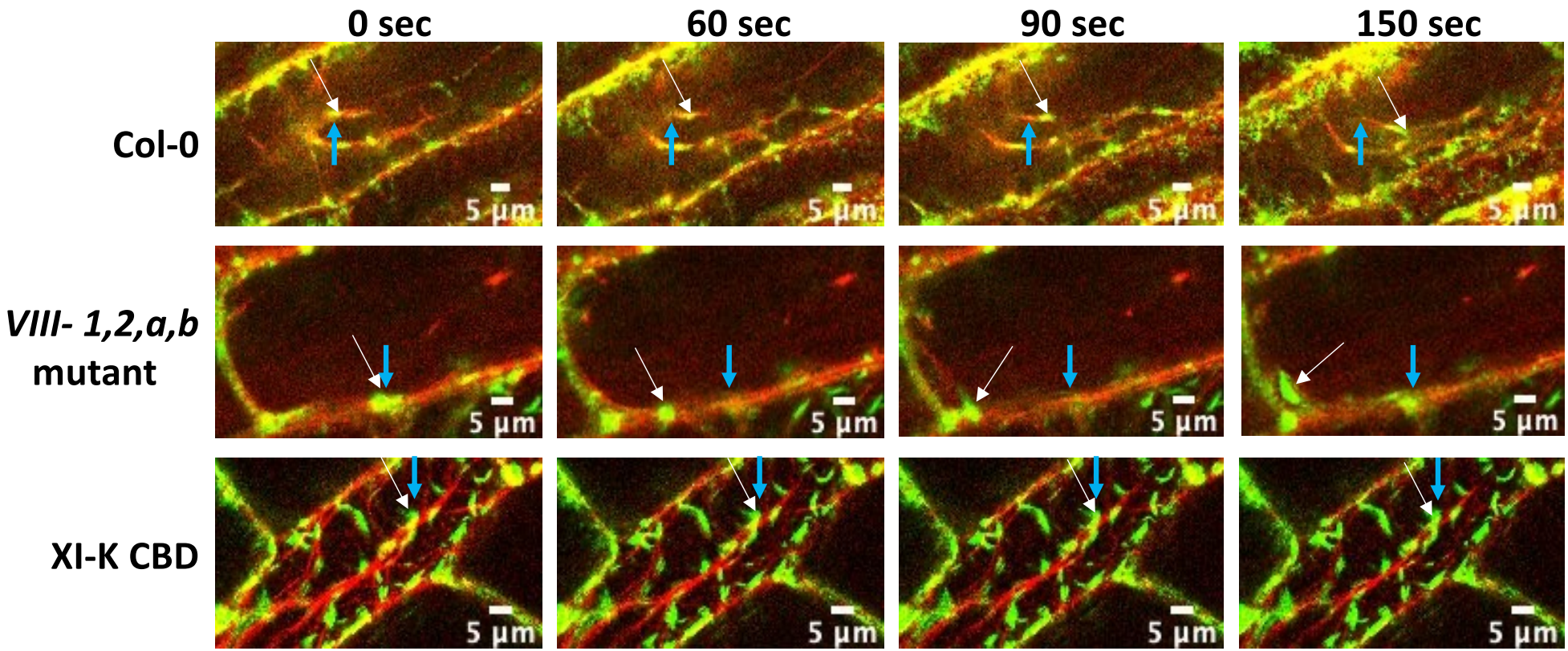

Figure 12. Loss of function of myosin XI-K, but not myosin VIII, disrupts movement of VirE2-Venus along actin filaments. Transgenic plants expressing mCherry-ABD2 constitutively and VirE2-Venus inducibly in Col-0, *myosin VIII-1/2/a/b*, and myosin XI-K CBD plants were used in this experiment. Roots of these plants were treated with 10 µM β-estradiol for 8 hr. Time lapse images were taken by confocal microscopy. Four images of each field are shown at the indicated times (0, 60, 90, and 120 seconds). Blue arrows indicate the initial position of a particular VirE2-Venus aggregate; white arrows indicate the position of the same aggregate at various times thereafter. Bars indicate 5 µm.

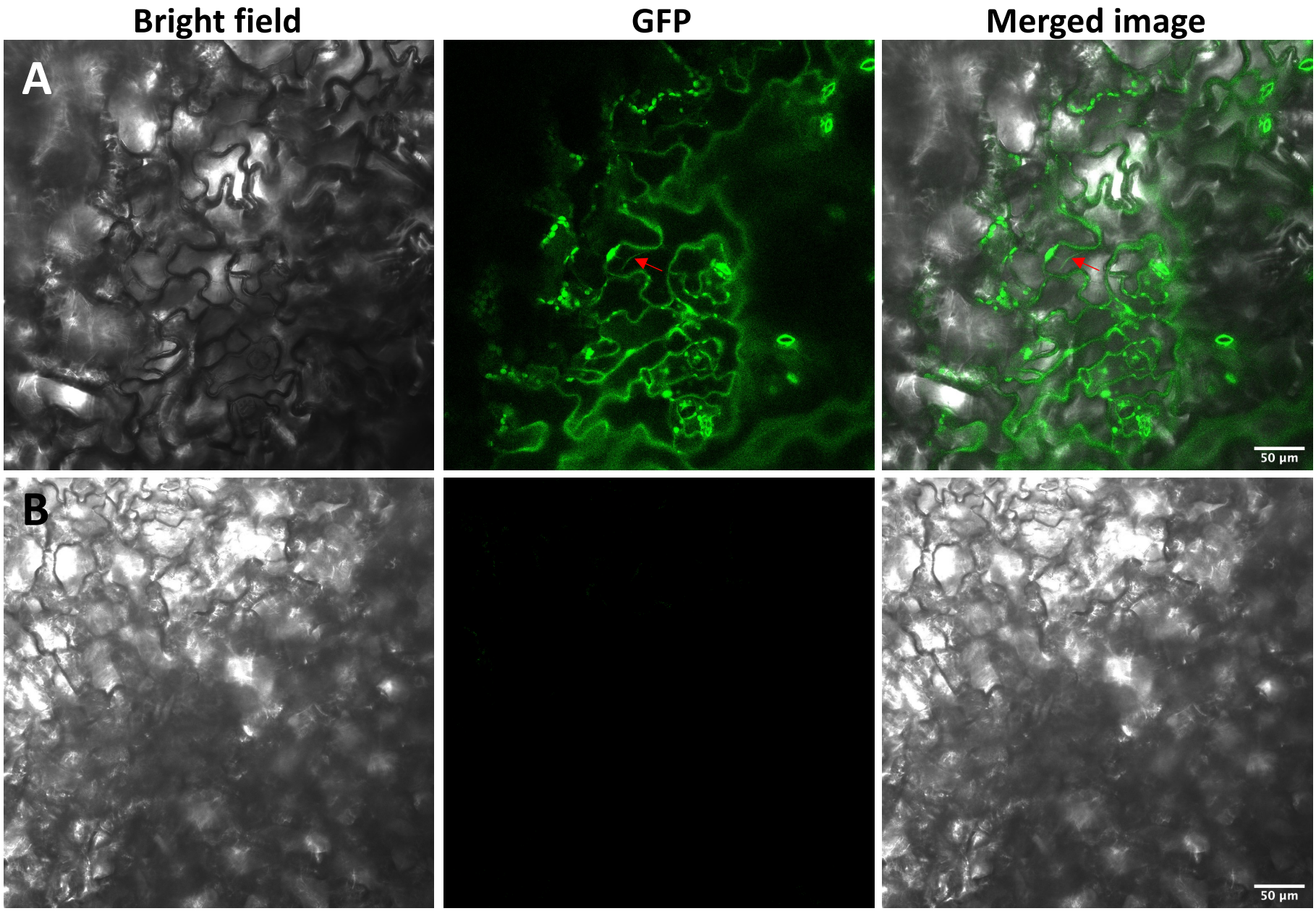

Figure 13. **VirE2-iGFP11 delivered from *Agrobacterium* localizes to the periphery of *Arabidopsis* cells and along filaments. (A)** *Arabidopsis* leaves expressing GFP1-10 were infiltrated with an *Agrobacterium* strain expressing VirE2-iGFP11. The leaves were imaged one day later by confocal microscopy. **(B)** Non-infiltrated leaves of *Arabidopsis* expressing GFP1-10. Red arrows indicate VirE2 along cytoplasmic filaments. Bars indicate 50 µm.

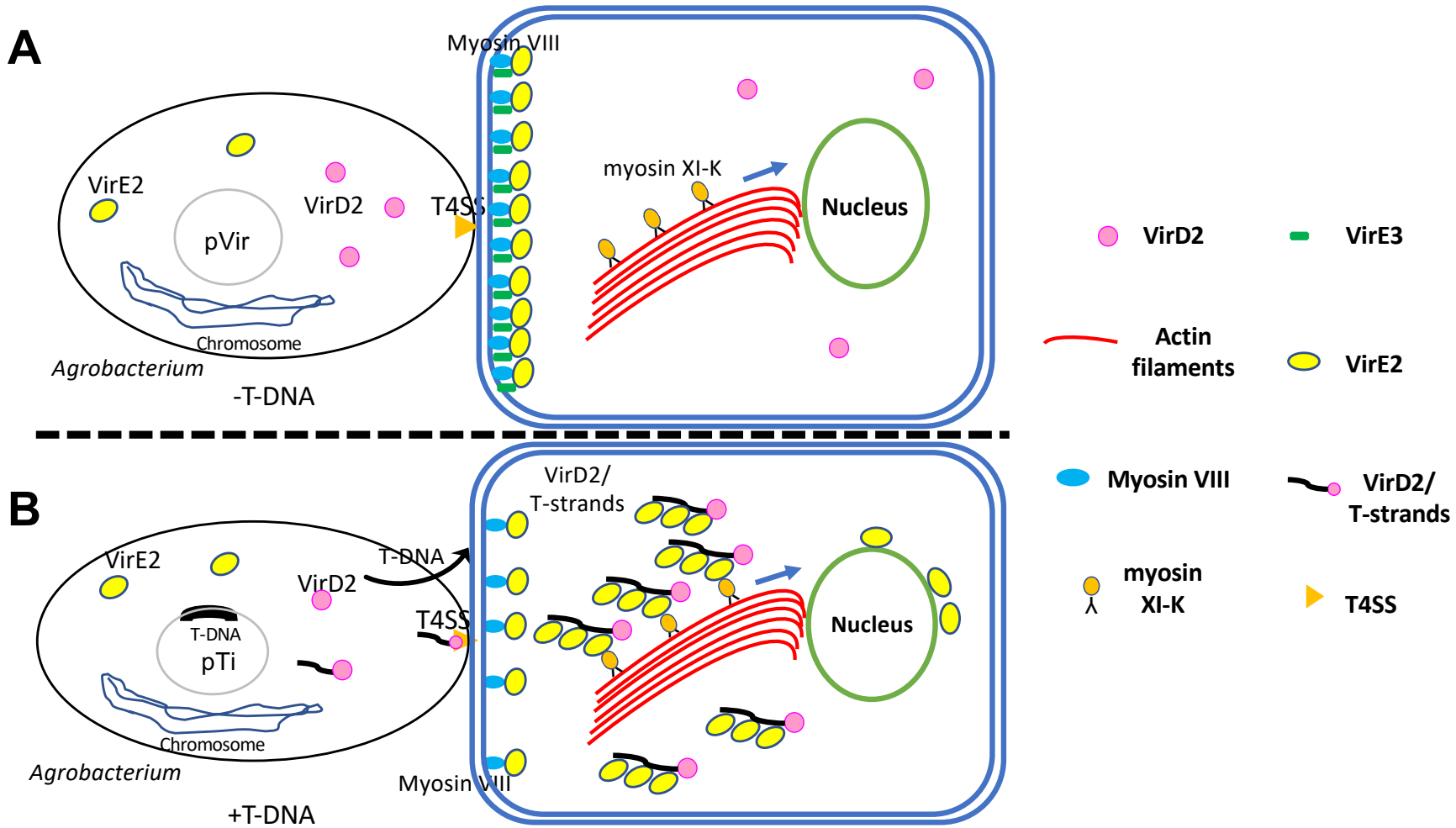

Figure 14. **Model of myosin VIII and myosin XI-K involvement in VirE2 trafficking to the perinuclear region. (A)** *Agrobacterium* virulence effector proteins, including VirE2 and VirE3, are secreted into host cells through a Type IV secretion system. VirE2 and VirE3 interact at the plant plasma membrane. Myosin VIII proteins localize at the plasma membrane and help tether VirE2 to the plasma membrane when no T-DNA is present. **(B)** When T-strands (as a VirD2/T-strand complex) enter the host cell, VirE2 molecules are released and some may bind T-DNA, following which VirE2 interacts with myosin XI-K and moves along actin filaments to the perinuclear region. Not shown are the *Agrobacterium* virulence effector proteins VirD5 and VirF which also are transferred to the plant.